THE INFLUENCE OF FABRICATION SCHEDULES ON THE FATIGUE LIFE OF X-60-W STEEL

A THESIS

Presented to

The Faculty of the Division of Graduate

Studies and Research

by

Alan Norwood Jackson

In Partial Fulfillment

of the Requirements for the Degree

Master of Science

in Mechanical Engineering

Georgia Institute of Technology

June 1972

In presenting the dissertation as a partial fulfillment of the requirements for an advanced degree from the Georgia Institute of Technology, I agree that the Library of the Institute shall make it available for inspection and circulation in accordance with its regulations governing materials of this type. I agree that permission to copy from, or to publish from, this dissertation may be granted by the professor under whose direction it was written, or, in his absence, by the Dean of the Graduate Division when such copying or publication is solely for scholarly purposes and does not involve potential financial gain. It is understood that any copying from, or publication of, this dissertation which involves potential financial gain will not be allowed without written permission.

_____

_____

7/25/68

THE INFLUENCE OF FABRICATION SCHEDULES ON

THE FATIGUE LIFE OF X-60-W STEEL

Approved:

Chairman

Date approved by Chairman: 6/26/72

ACKNOWLEDGEMENTS

The author wishes to express his appreciation to the many individuals who aided him in the successful completion of this investigation. Much appreciation is owed to the Republic Steel Corporation whose personnel made possible the fabrication program. Particular thanks are due Dr. A. B. Blocksidge, Jr., Assistant Director of Research, Dr. C. B. Griffith, Chief Metallurgical Development Section, and Mr. U. B. Gammon. Also, the comments of Dr. T. A. Davenport were appreciated.

The author is grateful to Dr. S. P. Kezios, who offered his assistance with the demise of Dr. Clough. Dr. B. G. LeFevre and Dr. J. H. Murphy are due a special note of thanks for their sincere interest and constructive comments as readers. Appreciation is also expressed to Dr. J. M. Bradford and Dr. E. E. Underwood who offered advice on several occasions. The assistance offered by Mr. J. Jakobsen was especially appreciated. Messrs. R. G. Grim, B. L. Wallace and H. J. Carr gave valuable advice during the machining operations.

The writer would like to express his gratitude to his wife, Jane, for her patience, understanding and encouragement during some trying periods in the development of this thesis.

This thesis is dedicated to the memory of Dr. W. R. Clough. He originally suggested this topic and guided the author in the initiation of this investigation. His instruction, example and inspiration were essential for its successful completion.

TABLE OF CONTENTS

TABLE OF CONTENTS (Concluded)

LIST OF TABLES

LIST OF ILLUSTRATIONS

LIST OF ILLUSTRATIONS (Concluded)

SUMMARY

With the increasing realization that significant alloy property improvements are not obtained by composition modification alone, much emphasis has of late been given to the examination of process-structure-composition interactions. Research recently completed by Y. M. Ebadi (single addition "Mn" high-strength low-alloy steel), by M. R. Pereyra (triple addition "Mn, V, Cu" HSLA steel) and by S. A. Andrew (double addition "Mn, Cb" HSLA steel) have shown that some mechanical properties of structural steels are strongly influenced by changes of fabrication temperatures at the hot mill. The objective of this investigation is to determine the influence of fabrication schedules on the fatigue life of this double addition HSLA steel designated by Republic Steel Corporation as X-60-W. Plate samples in an initial hot worked condition were hot rolled at several temperatures with the single phase austenitic field, at several temperatures within the critical range, and at several temperatures below the eutectoid temperature. The effects of changes in fabrication variables on microstructure were investigated by optical and transmission electron microscopy and related to variations of the determined fatigue limits. A rotating-beam fatigue machine of the "R. R. Moore" type was used to conduct all fatigue tests.

It was concluded that warm-rolling below 1250^{o}F resulted in enhanced fatigue strength which was directly proportional to the kinetic

parameters of recovery. Rolling at temperatures greater than the eutectoid temperature resulted in slight decreases in the fatigue strength of X-60-W steel as compared with the commercial as-rolled condition. These decreases are attributed to the relief of coherency stresses associated with the extremely small columbium carbides precipitated in ferrite during commercial production. Very good linear correlation was shown between the fatigue limit and surface hardness, ultimate tensile strength and yield strength. Rowe's method to predict the fatigue limit for steels, based upon the strain hardening exponent and strength coefficient as determined by a simple tensile test, satisfactorily predicted the fatigue behavior of X-60-W steel.

CHAPTER I

INTRODUCTION

Statement of the Problem

Structural steels are normally produced in the hot rolled condition in many common forms, as plate, sheet, strip, bar and bar shapes, and structural shapes. The production process for all forms is similar; a general description of the production of structural shapes will be given. A typical mill receives steel blooms from the blooming mill at 1800°F and charges them into furnaces where they are heated to about 2250°F in approximately 45 minutes. The blooms are then drawn from the furnace and rolled to the desired shape by rapid passage through breakdown, roughing, intermediate and finishing roll stands. In normal practice, all hot rolling is performed while the steel is in the temperature range of 1700-2200°F, which is within the single phase autenitic region. After hot rolling, the structural shapes are air cooled, then passed through straightening rolls, and finally, cut to size (1). Structural steels are seldom subjected to hardening heat treatments, but are usually used in the as-hot-rolled condition. Steels meeting the same composition limits and produced by the same processes (i.e. basic oxygen furnace, basic open hearth furnace, etc.; rimmed, killed, semikilled, etc.) will then have a set of mechanical properties which will show but little variation from heat to heat or producer to producer.

The material properties which must be considered by the design engineer must include the fatigue behavior, especially if the designed structure will be subjected to alternating stresses. All metals, when subjected to alternating stresses, are known to fail at stress levels which would be safe if applied unidirectionally. However, most steels exhibit a "fatigue limit," or maximum stress level below which the steel may be alternately stressed indefinitely without failure. Steels commonly exhibit a fatigue limit which is 40 to 60 per cent of the static ultimate tensile strength for polished specimens tested in rotating-bending (2). In recent years it has become increasingly apparent that significant property improvements are not obtained by composition modification alone, and much emphasis has been placed upon the examination of process-structure-composition interactions.

This investigation was primarily undertaken to investigate the possibility of improving the fatigue properties of a high-strength low-alloy steel by altering the final commercial mill hot rolling procedures.

For this study, a commercial high-strength low-alloy manganese-columbium addition steel which met ASTM specification A 572, Grade 60 was chosen (3). Steel from a production heat was supplied by the Republic Steel Corporation under their trade designation of X-60-W. A series of thermomechanical treatments was designed which included fabrication at several temperatures within the single phase austenitic region (two phase austenite-ferrite range), at several temperatures within the critical region and at several temperatures within the two

phase ferrite-cementite range below the eutectoid temperature. A rotating-beam fatigue machine of the "R. R. Moore" type was used to conduct all fatigue tests. The effects of changes in fabrication variables on microstructure were investigated by optical and transmission electron microscopy and related to variations of the determined fatigue limits with final processing temperatures.

High-Strength Low-Alloy (HSLA) Steels

HSLA steels are essentially structural steels with small alloying additions to achieve enhanced mechanical properties (4). They are often categorized on the basis of their minimum yield points which range from 35 to 80 ksi. By contrast, structural plain carbon steels exhibit yield points of 30 to 36 ksi. HSLA steels are used for applications where their slightly greater price is economically justified either by total structure weight reductions, increased durability, or increased corrosion resistance.

Carbon is the primary strengthening addition in HSLA steels as in all steels due to the ability of carbon to be almost entirely precipitated as metastable iron carbides. However, the strengthening mechanism due to carbon yield a corresponding decrease in steel toughness and weldability for each increment of additional strength. In general, the weldability of steels has been found to be determined by the following formula (5):

$$\text{Carbon Equivalent} = C + \frac{Mn}{6} + \frac{Cr}{10} + \frac{Ni}{20} + \frac{Cu}{40} - \frac{Mo}{50} - \frac{V}{10} \qquad (1.1)$$

where the concentration of each element is in weight per cent. The upper composition limits of the stronger weldable grades of plate steels correspond to a carbon equivalent of about 0.6 per cent. However, with proper control of welding variables, steels with higher carbon equivalents can be satisfactorily welded without preheat (6).

Manganese is a solid solution strengthener and grain refiner. It has a beneficial effect upon toughness and is often added to counteract the detrimental effect of some other alloying addition upon this property. Manganese is added to most HSLA steels. Nickel has a similar effect to those of manganese. Copper is added primarily for its beneficial effects upon corrosion resistance. Several copper addition HSLA steels possess four to six times the corrosion resistance of normal structural steels, and are often used in atmospheric applications without painting. Also, corrosion exposure tests have shown that paint coating applied to corrosion-resistant HSLA steels exhibit a longer service life. Vanadium and columbium (niobium) are used as alloying additions for their carbide strengthening and grain refinement properties (6). Vanadium and columbium addition steels now account for most shipments of the grades of steel classified as HSLA types (7).

Metallurgical Characteristics of Ferritic-Pearlitic Steels Containing Manganese and Columbium (Niobium) Additions

Manganese has long been added to steels for its grain refining characteristics (8). It hardens the ferrite by substitudial solid solution hardening. However, the rate of strengthening with amount of

added substitutional solid solution hardening element is not large. Therefore, this is an expensive way of strengthening steel (9). Manganese is considered an "austenite former," i.e., it reduces the temperature at which austenite is stable and causes the eutectoid composition to shift to lower percentages of carbon (10). This eutectoid composition shift results in an increase in the percentage of pearlite in manganese addition steels. The presence of manganese below 1.5 weight per cent causes a decrease in the impact transition temperature which cannot be attributed solely to the decrease in microstructural grain size. Phillips attributes this larger temperature decrease as due to the increase in the pearlite percentage and decrease in the pearlite laminar spacing caused by manganese (11).

Columbium is a very effective precipitation hardener of steel. Columbium has a very high affinity for carbon and a relatively low affinity for oxygen. The former property leads to its strengthining effects, the latter to its practical importance as a high percentage of the expensive columbium alloying additions added in the ladle is recovered in ingots of semi-killed steels (12).

The columbium precipitate in steel is frequently referred to as a columbium carbonitride. Electron diffraction studies have shown that the precipitates are either columbium carbide, nitride, or since these compounds are miscible; carbonitride. Studies on columbium addition steels in the as-rolled and normalized conditions revealed that these steels all strain-aged, indicating the presence of free nitrogen. These results lead Morrison to conclude that the precipitates are essentially columbium carbide (13).

The Petch equation is perhaps the most successful attempt to quantify the relationships which govern the properties of structural steels. This equation is (14):

$$\sigma_y = \sigma_o + kd^{-\frac{1}{2}} \qquad (1.2)$$

In the Petch equation, σ_y is the lower yield stress, $d^{-\frac{1}{2}}$ is the reciprocal square root of the mean grain diameter, and σ_o and k are material constants. The frictional stress term, σ_o, is that stress needed to move a dislocation through the lattice. It is a measure of the stress required to drive a dislocation against the resistance offered by impurities, precipitate particles, subgrain boundaries, the Peierls-Nabarro force, and other obstacles to dislocation motion. The frictional stress is a function of composition, prior metallurgical history, and of temperature. The second constant, k, is a grain boundary locking term. It is a measure of the concentrated stress required to unlock a dislocation where a slip band is held up by a grain boundary. It is essentially independent of temperature.

The effects of columbium carbide precipitates upon the strength of steel are two-fold. First, an extremely fine, coherent precipitate present in the ferrite matrix will be effective in raising the frictional stress term of the Petch equation and thus will raise the yield stress. Larger, incoherent precipitates of 300 Å or more are ineffective in raising the frictional stress term. However, they have a large effect upon final grain size as they are effective in retarding

recrystallization and grain growth of austenite (15). Controlled rolling of austenite below a temperature where columbium carbides begin to coarsen is effective in the production of fine-grained austenite which, upon transformation, yields fine-grained ferrite (16). It is well known that the strength and impact transition temperatures of fine-grained steels are superior to those possessing coarse grains.

The relative effects of columbium are greatest for steels which contain the least carbon (17). However, the presence of nitrogen or carbon is necessary for columbium to have a strengthening effect, as tests on steels from which essentially all the carbon and nitrogen were removed have shown (14). Columbium alters the morphology of cementite in pearlite as the cementite laminars in such columbium addition steels tend to acquire a granular shape (17).

Columbium carbides are exceptionally stable. The finer precipitates begin to dissolve and go into solid solution in austenite when heated to 1000°C (1832°F). However, long austenitizing at 1100 to 1200°C (2012 to 2192°F) is normally necessary to place all columbium carbides in solution (16).

Precipitation strengthened columbium addition steels retain their strengths even when heated to temperatures close to the ferrite-austenite transformation temperature. Morrison reported that a 0.15 weight per cent columbium steel which contained both coherent and incoherent columbium carbides maintained its hardness up to 100 hours at 700°C (1292°F). He concluded that there is an almost instantaneous loss of hardness when the ferrite transforms to austenite. This drop

is associated with the relieval of stress around the coherent precipitate in the ferrite matrix. Upon transformation to austenite, the precipitate acts as the nucleus for the growth of a stable incoherent particle which is effective for grain growth restriction, yet ineffective to influence the frictional stress (14). However, it is not until 1000°C (1832°F) is exceeded that the smaller incoherent precipitates begin to go into solution and the larger ones appreciably coarsen and coalesce so that they are no longer effective in restricting grain growth. If coarse austenite thus formed were slowly cooled to room temperature, coarse ferrite and pearlite would be obtained. However, coherent, extremely small columbium carbides would reprecipitate in the ferrite and act to raise its frictional stress (16).

It is now appropriate to ennumerate the three mechanisms by which columbium carbide precipitation occurs in steel which has been solution treated and continuously cooled (14,18).

First, if cooling is sufficiently slow, precipitation of relatively massive incoherent columbium carbides of 200-300 Å size will occur in the austenite. These particles are too large to strengthen the later formed ferrite. However, they are extremely effective in lowering the transformation temperature and restricting grain growth. The introduction of rolling during cooling through the austenitic range greatly increases precipitation of these large precipitates.

Secondly, as the steel is cooled into the two-phase austenite-ferrite range, "row-precipitation" of fairly large precipitates of greater than 50 Å may occur at the advancing austenite-ferrite interface.

This is an example of a discontinuous precipitation process described as autocatalycic. Gray and Yeo state that,

> Nucleation and growth occur in a reaction front (interface) that provides sites that can catalyze nucleation and growth as it moves into the super-saturated solid solution and thus leaves a two-phase aggregate behind. A prerequisite for the occurrence of discontinuous precipitation is that the reaction front must be able to sweep through the crystal before nucleation on sites in the matrix can take place (18).

Spretnak, in a discussion of Gray and Yeo's work, added that there is evidence that the austenite-ferrite interface propagates with intermittent jumps and rest periods, and that the jumps very likely advance with speeds the magnitude of sound. The rest periods thus become the predominant factor in controlling the over-all kinetics of the interface motion and supply sufficient time for nucleation and diffusion of the columbium carbide particles at the interface (19). These "row precipitates" are coherent, but due to their relatively large size (greater than 50 Å), they do not give the maximum strengthening possible form columbium additions.

Finally, a third mechanism is possible for columbium carbide precipitation. At lower temperatures, below the A_1 line, exceptionally fine, coherent precipitates of 20 to 50 Å size are formed. These precipitates are uniformly dispersed in the ferrite and are very effective in strengthening the ferrite by acting as barriers to dislocation motion and thus raising the frictional stress term of the Petch equation. Due to their small size, these precipitates are difficult to resolve, even by electron microscopy techniques.

Fatigue of Metals

The application of reversed or cyclic stress to metals can cause eventual failure even at stress levels where the metal would exhibit elastic behavior for unidirectional stressing. Failure of metals under the application of alternating stress is known as fatigue and is defined as the process of progressive localized permanent structural change occurring in a material subjected to conditions which produce fluctuating stresses and strains at some point or points and which culminate in cracks or complete fracture after a sufficient number of fluctuations (20).

A most simplistic description of the fatigue process is the following. Microscopic cracks are formed early in the fatigue life and almost always at the surface. Eventually, by a process of crack linking and progression one crack will become dominate. Further stress reversals will cause the dominate crack tip to progress until the part is no longer capable of withstanding the applied stress for even one more cycle. When this occurs, the part fails suddenly.

Due to the manner in which fatigue progresses, the appearance of a fatigue failure of a steel part can be divided into two distinct regions. The first region will be that of crack initiation and slow propagation. It will exhibit a smooth appearance which can be explained by the rubbing action of the free crack surfaces during each cycle of reversed stress. If the part has undergone variable stress amplitudes, the crack may stop under low stress and then continue when it later rises. This alternation of periods of slow or no growth

alternating with periods of fast crack growth changes the degree of rubbing experienced by the crack free surfaces and may result in what is termed a "clamshell" appearance of the smooth region. The second region is that of final failure. It experiences no cyclic rubbing action and usually has a coarse granular appearance. It is frequently necessary to use low power magnification in order to see any evidence of plastic flow. The fact that fatigue is the most common means of failure in machine parts, that it occurs at low stress levels which are considered safe for static loading, that it exhibits little evidence of ductile flow, and that the final failure region has a granular or crystalline appearance lead to the erroneous belief which still persists among laymen that metals "crystallize" in service and become embrittled (21).

The results of rotating-benging fatigue tests are usually presented as S-N diagrams which are semi-log plots of stress amplitude versus log cycles to failure. A well known feature of such diagrams is a rapid increase in specimen life when the test stress amplitude falls to some low level within the static elastic range. This area of the curve is known as the "knee." It is significant the for steels, the lower portion of the S-N diagram becomes horizontal and exhibits some limiting level of stress below which specimens will not fail if the test is continued for finite lengths of time. The maximum stress level is known as the "fatigue limit." Other metals do not demonstrate fatigue limits. Rather, the stress necessary to produce failure continues to decrease at a low rate with an increasing number of cycles.

The lack of a fatigue limit does not preclude the application of nonferrous materials in engineering designs, nor does it prevent an engineer from using a steel above its fatigue limit. Aircraft structural parts are commonly designed for high stress applications and removed from service at some fraction of their expected life, the exact service life being a matter for engineering judgment.

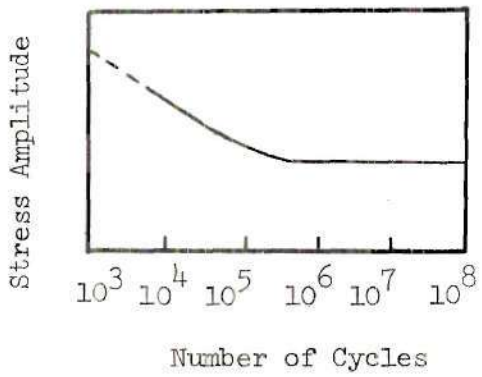

Figure 1. Typical S-N Diagram for Mild Steels

The knee of the S-N diagram usually occurs between 10^5 and 10^6 cycles for steel specimens. Analysis of the large number of references to rotating-bending fatigue testing of polished steel specimens reveals that the percentage ratio of the endurance limit to ultimate tensile strength varies from 40 to 60 per cent. It has long been established that tempered martensitic steels possess the higher ratios, whereas ferritic and ferritic-pearlitic microstructures more commonly exhibit

ratios of 50 per cent (2).

The occurrence of two distinct regions on S-N diagrams has prompted investigators seeking to elucidate the basic mechanisms of fatigue into considering them as possibly the results of different mechanisms. These two regions are commonly referred to as "High-Strain, Low-Cycle" fatigue and "Low-Stress, High-Cycle" fatigue. It is significant that the present empirical formulations which predict fatigue life are presented by their authors as applicable to only one or the other of these S-N diagram regions.

It is well established that the fatigue properties of metals are statistical in nature. It has long been known that at stress sufficient to cause failure within a finite number of test reversals that a considerable amount of experimental scatter in fatigue life is observable. This scatter generally increases in direct proportion to the proximity of the stress amplitude to the fatigue limit. At stresses only slightly above the fatigue limit, it is not uncommon to obtain fatigue lives which vary by a factor of 50 (22). It is not as well known that the fatigue limit also exhibits a considerable amount of statistical variability. Ransom and Mehl have shown that for transverse specimens of 4340 steel tested in rotating-bending, a mean fatigue limit of 46,270 psi with a standard deviation of 2900 psi was obtained. Longitudinal specimens from this same barrel had a mean fatigue limit of 67,040 psi with a standard deviation of 1,700 psi. The data quoted was the extreme case for their determination of fatigue properties of steels taken from four gun barrels. However, the standard deviations found serve to dramatize a variability of the fatigue limit which was not

previously appreciated. It is interesting to note that the yield strength for this steel was 107,000 psi, its ultimate tensile strength was 125,000 psi, and that these values were the same for both longitudinal and transverse specimens (23).

Generally, the fatigue strength is less for transverse as compared with longitudinal specimens, although the relative difference is seldom as large as in the above example. This directionality difference results from elongation of inclusions in the rolling (longitudinal) direction. Transverse specimens thus have elongated defects perpendicular to their major stress axis and a favorable crack initiation site exists (24).

Inclusions are detrimental to the fatigue strength of metals. They serve as preferential initiation sites for cracks and effectively increase the statistical scatter of fatigue data (25). Aksoy has demonstrated that for AISI 4340 steel the endurance limit is higher for vacuum melted specimens as compared with air melted specimens (26). Also, Moore reported extensive studies which demonstrate a definite increase in the fatigue limit for specimens of less than one inch diameter. These observations can be directly related to the effect of inclusions. Vacuum melted steels possess considerably less inclusions; the probability of obtaining a specimen with an inclusion at the surface would increase in indirect proportion to specimen diameter. Such behavior is analogous to Griffith's classical work on the strength of brittle solids.

The condition of the surface has a strong effect on a fatigue

strength. A specimen with a polished surface will exhibit a higher fatigue life than one which has simply been turned in a lathe. Any design feature which will serve to raise the localized tensile surface stress can be effective in decreasing the fatigue life. Analysis of the effects of the cyclic stresses in rotating-bending fatigue reveals that surface tensile stresses are harmful, surface compressive stresses are not. This knowledge is frequently employed by shot blasting critical parts to produce compressive stresses in the surface layers (21).

The fatigue process is generally considered to occur in ductile metals in three stages:

(1) crack initiation,

(2) crack propagation, and

(3) fracture.

If the surface of a specimen is electrolytically polished and the fatigue test is periodically stopped, definite changes of the surface will be observable. (Flat specimens tested in push-pull fatigue are best suited for these observations). After a time slip markings appear as sets of parallel slip bands within single grains which intensify with further stressing. These bands are found to vary in width and number dependent upon the stress level. Some of these slip bands will intensify and become persistent, that is they will remain visible under the optical microscope even after the surface is repolished and etched. Thompson has demonstrated that persistent slip bands exist in O.H.F.C. copper after only five per cent

of the total fatigue life (27). With still further cyclic stressing, it has been proven that intrusion and extrusions form at the free surface in the persistant slip bands. These intrusions are the first formations of what can be considered a microcrack and have been observed to form as early as 1/10 of the total fatigue life. Once these intrusions or microcracks are formed, they grow from grain to grain (at the surface) and link up to finally form a dominant macroscopic crack. Investigations have shown that fatigue initiation is essentially a surface phenomena. The microcracks dc not penetrate further than a few grains deep. For low-stress, high-cycle fatigue, the total time to form the dominant microcrack is typically 90 per cent of the total time to fracture. The remaining 10 per cent is involved in crack propagation until the effective cross section is sufficiently reduced that catastrophic final failure occurs (28).

The appearance of these slip bands is significant in that they are concentrated, or coarse, which is opposite the nature of the appearance of slip in unidirectional stressing (29).

Crack initiation is essentially a surface phenomena, although there is evidence that in some instances fatigue cracks have initiated beneath the surface (30,31). There have been many reported experiments which extended the fatigue life, sometimes apparently indefinitely, by periodically removing as little as 20-30 microns from the specimen surface (32).

Hempel has reported observations on the formation of slip bands in a mild steel with 0.09 weight per cent carbon. The occurrence of

the first observable slip bands and their rate of propagation depended largely on stress level. At loads above the fatigue limit, the first slip bands could be seen after a few thousand cycles. The number and thickness of the slip bands steadily increased up to 4.6×10^7 cycles. A stress level 22 per cent below the fatigue limit revealed no slip bands even after 1.5×10^7 cycles. These observations are presented graphically below as Figure 2 (33).

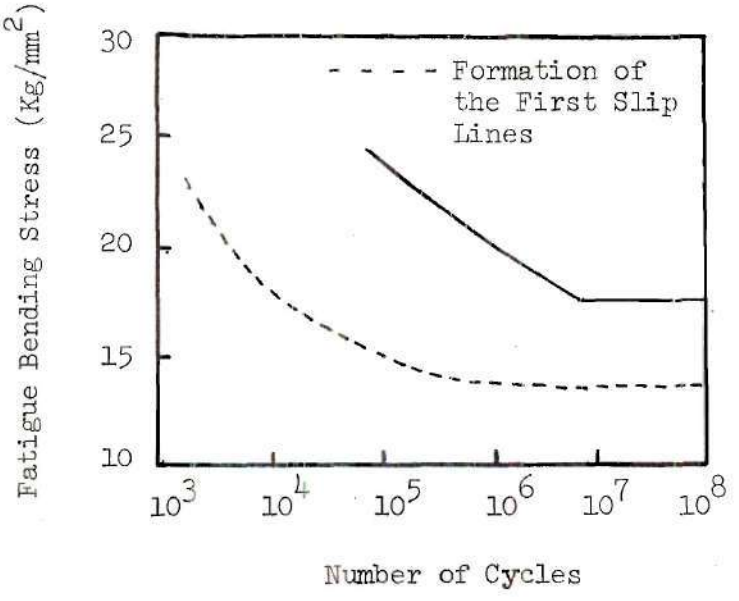

Figure 2. Occurrence of the First Slip Lines on Unnotched Flat Specimens of 0.09 Per Cent Carbon Steel.

For notched fatigue specimens of the same steel, Hempel found that slip traces did not differ from those of unnotched specimens.

However, the observable slip bands were confined to the immediate vicinity of the root of the notch and occurred at lower stresses due to the stress concentration there.

The crack propagation may be considered to be governed by the maximum principal stresses occurring at the crack tip. Fracture striations which are observable on the fracture surface through electron microscopy are formed and their spacing represents the crack advance per cycle. As mentioned earlier, the crack propagation stage commonly occupies about 10 per cent of the total life for low-stress, high-cycle fatigue, and is followed by sudden catastrophic failure. However, on tests of a low alloy cast steel tested at alternating stresses slightly above the fatigue limit, Nordbert and Aronsson found that crack initiation occupied roughly 99 per cent of the total life. Crack propagation accounted for only 1 per cent of the total number of cycles to failure (34). On the contrary, the process of crack propagation occupies a majority of the fatigue life for tests in the high-strain, low-cycle category. Also, for high strain fatigue the tendency is for intergranular cracking to occur in contrast to the transgranular cracking common to low-stress, high-cycle fatigue (35).

Generally, any method which strengthens the metal with respect to the relative ease with which slip can occur at the surface will result in an increase of fatigue life. The deformation of a metal is known to introduce strain hardening which is caused by the creation of dislocations and dislocation tangles in the grain sub-

structure. Consequently, it is no surprise that cold working a metal will increase its fatigue life (36). However, there is an optimum degree of cold working above which the fatigue strength is decreased. The increase in fatigue life for shot blasted parts has already been mentioned. Strain hardening in fatigue may be measured by observing the variation in stress necessary to produce a constant plastic strain amplitude in cyclic testing. In contrast to the behavior observed in unidirectional tensile tests, strain hardening saturates within the first 1 per cent of fatigue life (30,37). Thereafter cycling continues with little or no change in stress amplitude required. The strain hardening curve will rise sharper and saturate sooner for increasing levels of plastic strain amplitude. This behavior can serve as a mechanism to increase the fatigue limit in metals. It has long been known that stressing at low levels and progressively increasing the stress would significantly increase the fatigue limit (38).

If S-N diagrams prepared from tests run at different temperatures for the same alloy are studied, the only difference will be an observed increase in fatigue life with decreasing temperature. An exception occurs for steels and refractory BCC alloys susceptible to strain aging at specific temperatures and has been explained by Levy and Sinclair in terms of the diffusion of solute atoms to dislocations and to the consequent locking of such dislocations by the Cottrell atmospheres so formed (39). This mechanism has been disputed by recent Japanese research which found that the peak of fatigue strength versus

temperature curves is dependent upon interaction between carbide precipitates and dislocations rather than segregation of carbon and nitrogen atoms to dislocations (40). The similarity of the S-N diagram at all temperatures plus the fact that fatigue occurs at 1.7°K has been accepted as evidence that temperature dependent mechanisms such as surface corrosion, gas absorption or diffusion into the metal, or vacancy diffusion to form voids are not necessary for fatigue failure (41).

In general, finer grained metals are more resistant to fatigue than coarse grained ones. As grain boundaries represent obstacles to cracks advancing along slip bands this fact is not surprising (42). However, wrought ferritic steels do not usually demonstrate a correlation between fatigue strength and grain size. Teed emphasizes that it should be remembered that steel grain sizes are extremely small in comparison with most nonferrous alloys (43).

Methods to Predict Low-Stress, High-Cycle Fatigue Results

Rowe has presented empirical formulations based on true stress-true strain curves which predict the fatigue limits of materials tested in rotating beam fatigue (44). His method is the first attempt to quantitatively calculate the fatigue limit in terms of strength and work hardening. His predictions for steels generally agree within ±3000 psi. Rowe emphasizes that published fatigue data seldom includes sufficient data points to allow precise determination of the endurance limit for a probability of 0.5; therefore, published data should usually be regarded as possessing an uncertainty of several thousand psi. His equation for the fatigue limit with a probability

of 0.5 for steels is:

$$Se = 1.0139^{\frac{1}{n}} K^{0.911} \qquad (1.3)$$

Where n is the strain hardening exponent and K is the strength coefficient determined from the true stress-true strain curve. Rowe has also derived similar equations for the fatigue limit of notched steel specimens and for heat-treated aluminum alloys (fatigue limit based upon 5×10^8 cycles).

Esin has developed an analytical method which predicts fatigue failure and endurance limits for low-stress, high-cycle fatigue tests in excess of 10^5 cycles. His approach considers the fatigue process as a single stage process of energy conversion and is based upon a statistical approach to microplasticity (45). In the range where he considers his method as accurate, metals are normally considered elastic. It has long been established that in cyclic stressing, metals can undergo plastic flow on a microscopic level. Esin relates fatigue damage to the plastic hysteresis energy dissipated per cycle and assumes that fatigue fracture occurs when the accumulated plastic strain energy reaches the value under the true stress-true strain diagram. His necessary parameters were obtained from tensile tests by measuring the changes in the a-c resistance under strain in order to differentiate between elastic and plastic strain and to detect microplasticity. He presented experimental data which demonstrated good correlation with

this method for six steels tested in push-pull type fatigue machines. He concluded that:

1. Plastic strain energy can be used as a measure of the damage occurring in the fatigue process.

2. The accumulation of the plastic hysteresis energy to the value under true stress-true strain diagram is a reasonable criterion for fatigue failure as long as the fatigue process does not cause changes in the state of matter to the extent of altering the origin parameters on which the analysis is based.

3. The fatigue process, particularly in the long life region, is a very localized event; therefore, the damaging energy could not be represented by macroscopic parameters. This requires an approach to the mechanical behavior at microscopic level which involves a statistical treatment.

4. The microscopic properties of a material are dependent upon the microstructure which is so variable in nature that the statistical functions cannot be approximated by mathematical assumptions. Therefore, an experimental method is required to gain an understanding of the microscopic properties.

In summary, it has been stated that fatigue is a failure mode which occurs in three stages:

(1) crack initiation,

(2) crack propagation and

(3) final fracture.

The basic mechanisms which govern each of the three stages have not as yet been successfully explained. It is known that any mechanism which strengthens the metal, especially the surface, is beneficial to the fatigue life. The current best methods to predict fatigue failure are based on empirical determinations which are dependent upon the statistical response on a microscopic level for heterogeneous engineering materials.

CHAPTER II

MATERIAL, FABRICATION, AND SPECIMEN PREPARATION

X-60-W Steel

All steel tested in this study was from production heat no. 415855 of Republic Steel Corporation's designated X-60-W steel. It is a high-strength low-alloy steel with low level alloying additions of manganese and columbium, and belongs to an alloy class of ferritic-pearlitic steels upon which the first developmental work began about 1958 (46). The steel supplied for this testing program qualifies under ASTM Designation A 572, Grade 60 and is suitable for riveted or bolted construction of bridges, and for riveted, bolted or welded construction in other applications (3).

The advertised (47) minimum mechanical properties for X-60-W steel are presented in Table 1, along with the corporate determined actual properties for heat no. 415855 (48).

Table 1. Mechanical Properties of X-60-W Steel

	Yield Point (psi)	Tensile Strength (psi)	Elongation (per cent)
Advertised Minimum	60,000	75,000	18(in 2 in.)
Determined Value	63,165	86,760	18(in 2 in.)

All samples of X-60-W steel used for this investigation were taken from one plate. This plate was produced at Republic Steel's production facility in Gadsden, Alabama. The exact nature of the plate rolling schedule is corporate proprietary information. However, Republic Steel did reveal that the schedule involved some controlled rolling operations, including hot finishing. The analyzed chemical composition was 0.25 C, 1.1 Mn, 0.017 P, 0.017 S, 0.027 Si, 0.07 Cu, 0.04 Ni, 0.02 Cr, 0.011 Sn, 0.01 Mo and 0.023 Cb; all concentrations being on a weight per cent basis. An important assumption of this testing program is that the supplied steel was representative of X-60-W steel produced by the Republic Steel Corporation.

The Thermomechanical Treatment Program

A comprehensive fabrication program was developed by the late Professor Clough and performed at the Republic Steel Research Center in Cleveland, Ohio, by the acknowledged corporate research personnel. The included fabrication schedules were conceived to include all practical thermomechanical treatments which might result in enhanced fatigue properties of this commercially supplied low alloy structural steel. The designed heating and rolling schedules included the following treatments:

(a) High Temperature Thermomechanical Treatment (HTMT), which is deformation in the stable austenitic region, i.e., above the A_3 line (49). The austenitizing temperatures were such that they included intermediate temperature ranges where essentially all cementite was in solid solution, but the columbium carbides were only

partially dissolved or coarsened; and lower temperatures where the columbium carbides were essentially unaltered yet the cementite was dissolved.

(b) Isoforming, which is deformation which occurs simultaneous with transformation to pearlite in the metastable austenitic range below the A_1 line (50).

(c) Warm rolling after the material was heated to temperatures below the A_1 line where the first austenite would form. These temperatures were too low to be considered thermomechanical treatments.

Ten plate samples were taken from the mentioned X-60-W steel production heat for use in this fabrication program. Each sample plate was 10 inches long by six inches wide by a half inch thick. The length direction was in the mill rolling direction. This orientation was maintained for all subsequent experimental fabrication. The choice of plate sample size was dictated by the capacity of available furnaces adjacent to the rolling mill at the Republic Steel Research Center and by the capabilities of the research mill itself. The rolling mill was of two-high configuration, was reversing, had 14-inch diameter rolls of 20-inch effective length, and was operated at 1000 rpm during all controlled rolling experimentation.

One plate sample was given the numerical designation "1" and was set aside as representative of the commercial production heat. The nine remaining plate samples were respectively introduced into furnaces at 800, 950, 1100, 1250, 1400, 1550, 1700, 1850, and 2000^{o}F; were held in the furnace for one hour; and were then removed and as

rapidly as possible rolled to 0.32 inch thickness in two mill passes of 20 per cent reduction each. Only a few seconds elapsed between each of the two mill passes for each plate sample. To insure that all experimental plates received equivalent cooling, each sample plate was placed in a granular material specifically provided for cooling purposes immediately after exiting from the rolling mill. A numerical designation was given to each sample as indicated by Table 2.

Table 2. Numerical Designation of Fabrication Samples

Furnace Temperature (^{o}F)	Numerical Designation
Mill	1
800	12
950	13
1100	14
1250	15
1400	16
1550	17
1700	18
1850	19
2000	20

Preparation of Test Specimens

Fatigue Specimens

All fatigue test specimens were prepared in the Materials Processing Laboratory of the School of Mechanical Engineering, Georgia Institute of Technology, by the author of this investigation. Assistance

and guidance was given by acknowledged machine shop personnel. All machining operations were conservatively done in order to avoid localized heating which could alter material fatigue properties.

Specimen blanks approximately 3 1/2 inches long by 13/32 inches wide were cut from the plate samples. All cutting was done on a DoAll Metalmaster band saw with a blade of 1/4 inch depth and 14 teeth per inch. To identify its prior position in the sample plate, each blank was given a letter designation as indicated in Figure 3 or 4 and was placed in an envelope marked with the rolling temperature numerical designation and the specimen location letter designation.

The centers of the specimen blanks were determined by end mid-height marks scribed with a vernier height gage and punched with an automatic center punch. Each specimen was then placed in a drill press vice and its longitudinal axis was vertically alligned with a square prior to tightening the vice jaws. The vice, with the vertically alligned specimen, was placed on the table of a Clausing Series 16 VC-1 Drill Press, and the center was drilled with a no. 3 center drill. Drilling was slowly done in two stages. An initial cut was made until the flute of the drill began to cut. The drill was backed out; the hole lubricated with a light oil; and the cut was then continued until the top of the center drill bit flute was nearly buried into the steel. This completed drilling of one center hole. Next, a plate of steel was rigidly clamped to the table of the drill press, and a center hole was drilled into it using the same procedure as stated above. A 0.312 inch diameter steel ball was placed in this hole to

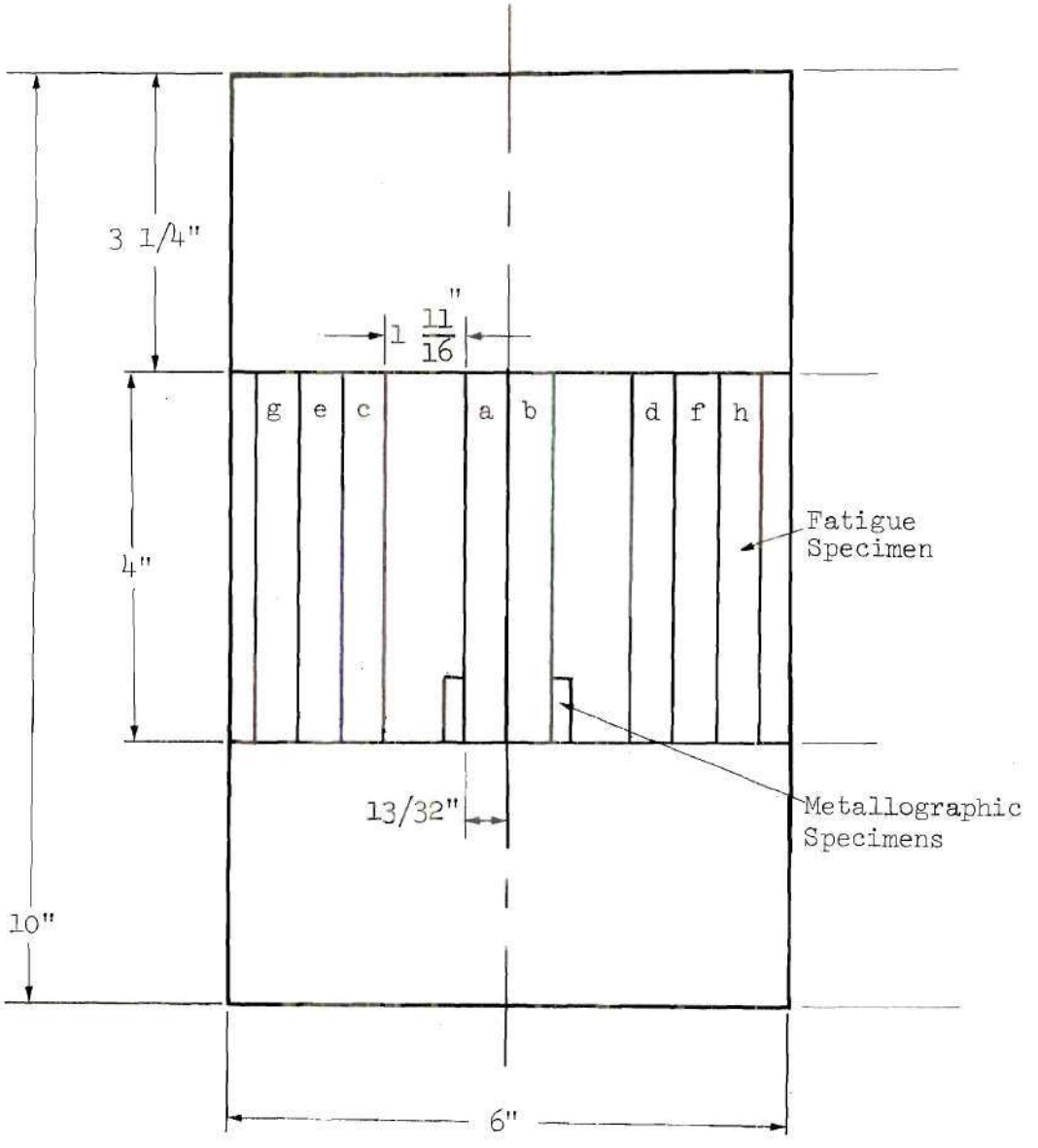

Figure 3. Location of Test Samples Relative to the Mill Condition Plate.

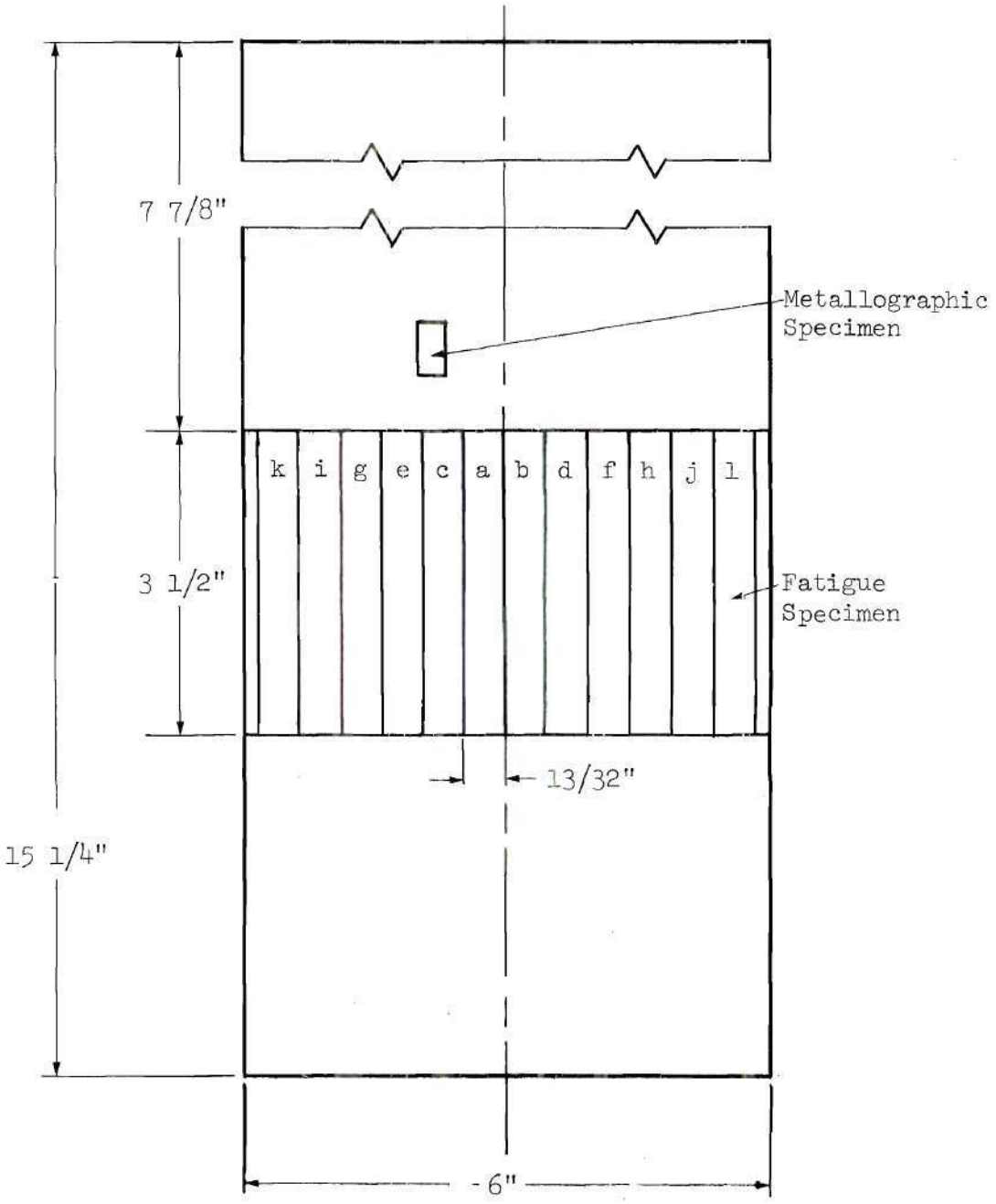

Figure 4. Location of Test Samples Relative to the Fabricated Plate.

serve as a point of support for the specimen blank as the second center was drilled. Next, the specimen blank was placed with its first center resting on the ball, and was gripped with vice grip pliers to prevent it from rotating. Finally, the drilling of the second center hole was performed in two stages as previously described. This method was chosen as a satisfactory procedure for achieving coaxial center holes for support of the specimens during the subsequent machining and polishing operations.

All specimen blanks were rough machined on a South Bend Quick Change Gear Lathe, Catalog No. 8187 AN. All cutting was done in the direction of the lathe head stock. After rough machining, the ends of the cylindrical specimens were accurately ground square and their lengths reduced to 3 7/16 inch in a Model No. B360 K.O. Lee Co. Grinder. Finish turning was done on a South Bend Precision Lathe, Model No. CL187RB. A feed of 0.0015 inch and a maximum final cut of 0.003 inches was used.

The gage section of each fatigue test specimen was turned in a Clausing Lathe, Model No. 6329, equipped with a True-Trace Mark 3 Series Lathe Tracer Attachment, Model No. 2057-01. Lubrication was supplied by a tool mist coolant generator which sprayed a water soluble cutting fluid. The final cut and feed were as before. Again, all cutting was in the direction of the lathe head stock. Dimensions of the test specimens were shown in Figure 5. These dimensions are in accordance with the testing machine manufacturer's recommendations. The 0.2400 inch shank diameter was necessary because the sample plate thick-

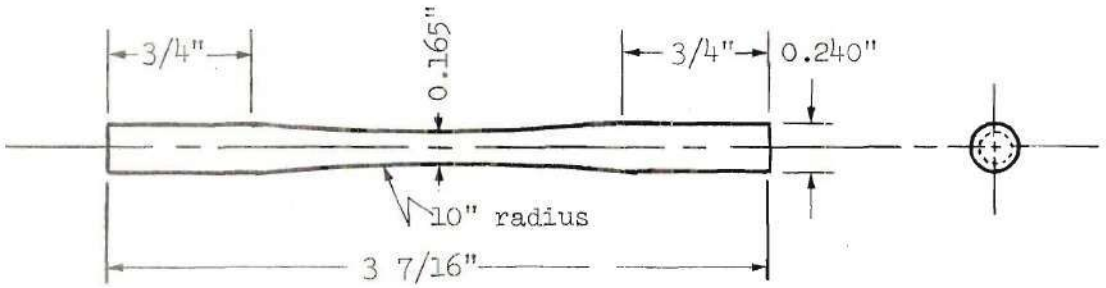

Figure 5. Fatigue Test Specimen Dimensions.

ness was only 0.320 inches after the 40 per cent reduction.

Polishing of the gage section was accomplished with the specimen rotating at 50 rpm in the South Bend Quick Change Gear Lathe. Aluminum oxide polishing cloth was wrapped around a rotating bar which was held lightly against the specimen and moved slowly in one direction with a uniform motion. The rotating bar was driven at 1750 rpm by a flexible shaft. This bar was held at an angle slightly less than 90 degrees to the axis of the specimen. By reversing the direction of rotation of the lathe for each new grade of polishing cloth, the scratches were generated at a different angle for each new polishing operation.

Polishing was accomplished in three stages: (1) with 120, (2) with 240, and (3) with 400 grit cloth. Polishing with the 120 grit cloth was continued until all visible circumferential scratches from the machining operations were removed. Polishing with the 240 and 400 grit cloths was performed with a liberal supply of kerosene being applied to the specimen. Each polishing stage was continued for approximately twice the length of time necessary to remove the scratches generated by the previous grade cloth. The edges of the polishing cloths were torn back at frequent, regular intervals in order to prevent the cloth from filling up and having a burnishing effect.

Immediately after polishing, each specimen was sprayed with a moisture displacive oil meeting government specification, MIL-C-23411. It was then sealed in a four inch long plastic tube of 1/4 inch inner

diameter, and returned to its individual envelope. MIL-C-23411 oil was reapplied to each specimen during any subsequent handling.

Metallographic Specimens for Electron Microscopy

The specimens which Mr. Andrew had prepared for optical microscopy by standard metallographic polishing techniques were also used for this investigation (51). Prior to replication, they were repolished with a 0.3 micron polishing solution and etched with a 2 per cent Nital solution. Specimen locations are as shown in Figure 3 and 4. The polished specimen surfaces lie in a plane defined by each plate's longitudinal (rolling) direction and its thickness. Specimen replication and electron microscopy was performed by Mr. J. L. Hubbard of the Georgia Tech Engineering Experiment Station. Two stage replicas, platinum shadowed at 30 degrees and backed with carbon, were employed for electron transmission microscopy utilizing a Philips EM200 Electron Microscope.

CHAPTER III

EXPERIMENTAL PROCEDURES

R. R. Moore Fatigue Testing Machine

All fatigue testing was performed using an R. R. Moore High Speed Fatigue Testing Machine manufactured by the Wiedemann Division of the Warner & Swasey Co. (now SATEC Systems, Inc.). This machine is of the pure-bending, rotating-beam configuration in which the test specimen functions as a simple beam symmetrically loaded at two points. When the specimen is at rest, fibers above its neutral axis are in compression and those below are in tension. Thus, for a specimen at rest, the maximum and minimum stresses are experienced by the outer most metal fibers of the bottom and top surfaces respectively. As the specimen rotates through a complete revolution, the test specimen passes through a complete cycle of flexural stress.

An R. R. Moore type machine is shown diagramatically in Figure 6. It consists essentially of two bearing housings, each of which contains a rotating spindle. One end of each spindle forms a tapered chuck which accommodates a tapered spring collet to grip the straight-shank specimen. Draw bolts extend through the spindles and, when screwed tightly into the collets, lock the specimen ends tightly in the spindles; thus forming a continuous simple beam supported on trunnion rollers at the outer ends of the bearing housings. Knife edge seats located at the specimen end of each bearing housing support knife edges mounted

Nomenclature

A Support Post

B Draw Bolt

C Bearing Housing

D Specimen

E Housing End Plate

F Trunnion Roller

G Flexible Coupling Assembly

H Motor

I Revolution Counter

J Loading Harness Assembly

K Base

L Spring Assembly

M Weights

N Load Pan

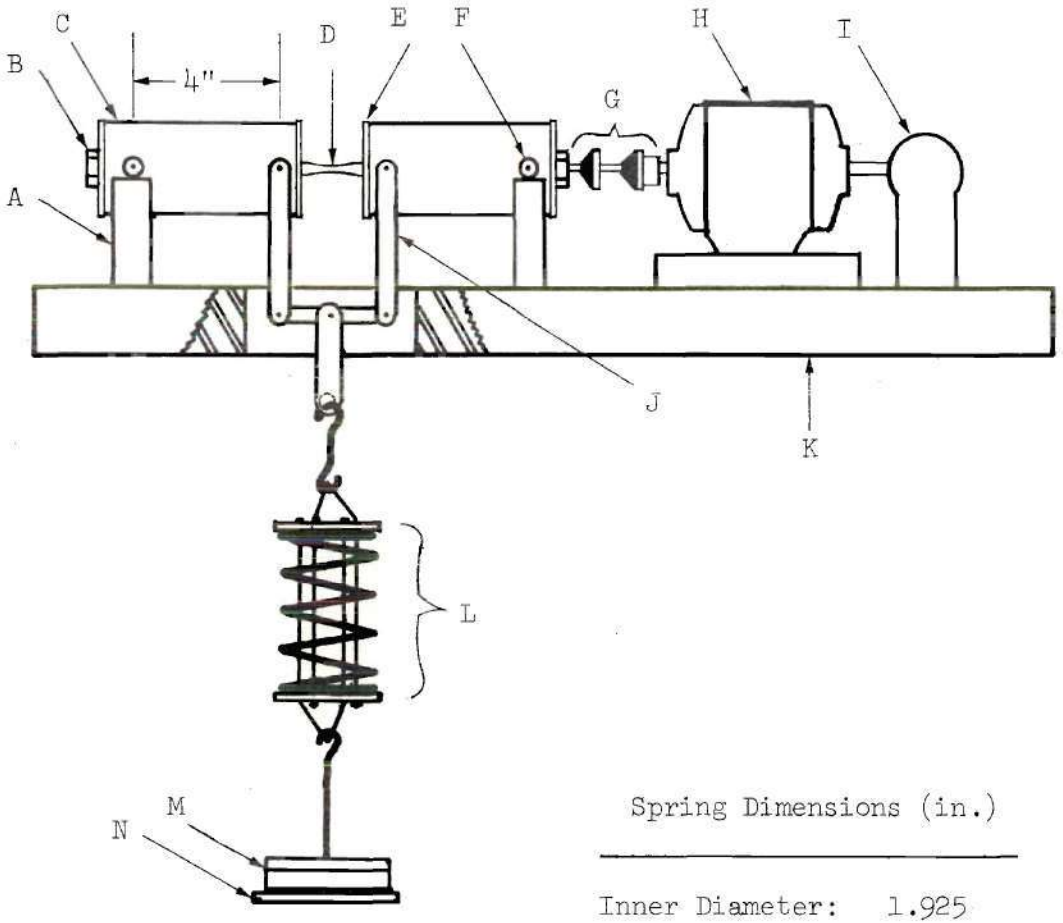

Spring Dimensions (in.)

Inner Diameter:	1.925
Wire Diameter:	0.125

Figure 6. R. R. Moore Fatigue Testing Machine.

in the yokes of the loading harness assembly. The fixed distance of four inches between the points of load application at the knife edge seats and the housing supports at the trunnion rollers insures uniform bending moment throughout the specimen test length. A compression spring assembly was designed and placed between the yoke and loading pan to incorporate resiliency in the loading system for the purpose of minimizing any inertia stresses resulting from small, unavoidable vibrations of the specimen and to aid in the gradual application of the load weights. The composite simple beam is rotated by means of a flexible coupling which offers no appreciable restraint to deflections of the housings. The high-speed motor operates at 10,000 rpm from the commercial source of 110 volts, 50 cycles AC power. A cutoff switch automatically stops the motor when the specimen breaks and prevents automatic restarting of the motor should the power temporarily fail. A resetable counter registers each 1000 cycles of stress up to one hundred million cycles.

The fatigue machine was leveled by shimming and bolted onto a heavy wooden table located in Room 108 of the Mechanical Engineering Building. This table rested on 1/2 inch thick rubber pads to lessen the transmission of vibrations from extraneous sources.

The effective weight of the bearing housings, draw bars and collets; plus the total weight of a typical specimen, the loading harness assembly, load pan, compression spring and hanger determined the minimum bending moment in the specimen. This total effective minimum load was statically determined as 6.56 lbs. The total effective load

on a specimen is the sum of this minimum effective load plus the sum of all weights stacked on the load pan.

Specimen Measurements

A Leitz Toolmaker's Model WMII Microscope was used to determine the specimen minimum diameter and the per cent deviation from true round. Each specimen was supported between center supports of the microscope. At the minimum cross section, two mutually perpendicular diameters were measured and their average reported as the specimen minimum diameter. Next, the specimen was rotated on the microscope centers and the diameter deviation at one side, as viewed through the microscope was determined and recorded. The per cent out of round was calculated as the per cent ratio of diameter deviation to average diameter. The values are reported in Table 4.

Machine Set Up and Starting Procedure

All dirt and rust was removed from the tapered holes in the spindles and from both inner and outer surfaces of the collets. Kerosene and 400 grit aluminum oxide polishing cloth were used when necessary. After the specimen, collets, housings and draw bars were assembled, the assembly was lifted and placed on the support posts as shown in Figure 5. Care was exercised during assembly transport to prevent strain on the specimen. The assembly eccentricity was determined with a Starrett Dial Test Indicator, Model No. 711. This eccentricity was measured at the top surface of each bearing housing's inner end plate. The assembly eccentricity was taken as the average

of these two measurements. Whenever it exceeded 0.0020 in., or vibration was noted after the motor was started; then the entire assembly was removed. One end was disassembled, and either the specimen or collet was turned a partial revolution while the spline was restrained. This procedure was systematically repeated until the desired tolerance was achieved. Average set up eccentricity for all tests was 0.0015 inches.

After the knife edges of the loading harness were seated, the motor was started. During all starting and stopping procedures, the bearing housings were hand supported to dampen vibrations which occurred as the beam assembly passed through its critical speed. After the motor had attained full speed, the hook of the loading pan, loaded with the desired quantity of dead weights, was lowered slowly onto the loading assembly spring. Finally, the revolution counter was set at zero. Each test was temporarily stopped after the first five and thirty minutes of testing in order that the draw bolt tightness could be checked.

Fatigue Tests

Fatigue tests were performed on a total of 72 specimens. The objective of fatigue testing was to determine the fatigue limit and shape of the S-N diagram for each of the 10 previously described steel conditions. At the onset of this investigation, it was realized that there was an insufficient amount of material available in order that a sufficient number of tests could be run to qualify the test results for statistical analysis. For example, only seven specimens could be prepared for the mill condition steel. Twenty test specimens are

considered to be the minimum population size for valid statistical analysis of fatigue test scatter (23).

For a specimen tested in a rotating-bending fatigue, the most damaging stress is the maximum tensile stress which is experienced at the bottom surface. The following standard nomenclature had significance for this investigation (52):

Stress Cycle - A stress cycle is the smallest section of the stress-time function which is repeated periodically and identically.

Maximum Stress - The highest algebraic value of the stress in the stress cycle, tensile stress being considered positive and compressive stress negative.

Minimum Stress - The lowest algebraic value of the stress in the stress cycle.

Range of Stress - The algebraic difference between the maximum and minimum stress in one cycle.

Alternating Stress Amplitude - One half the range of stress.

Mean Stress - The algebraic mean of the maximum and minimum stress in one cycle.

Fatigue Ratio - The ratio of the fatigue limit to the static tensile strength.

Stress Ratio, R - The algebraic ratio of the minimum stress and the maximum stress in one cycle.

Fatigue life, N - The number of stress cycles which can be sustained for a given test condition.

S-N Diagram - A plot of stress against number of cycles to failure.

Fatigue Limit - The limiting value of the stress below which a material can presumably endure an infinite number of stress cycles, that is, the stress at which the S-N diagram becomes horizontal and appears to remain so.

The stress experienced by any point in a specimen may be computed by the flexural formula for pure bending of a simple beam (see Appendix

A). For rotating-bending fatigue tests the mean stress is equal to zero. The stress amplitude can be shown to equal the absolute value of the maximum or minimum stress. As the minimum stress is compressive, thus negative by convention, the stress ratio R is equal to minus one.

The first test specimen for each condition was usually run at a stress amplitude of about 56 per cent of the average ultimate tensile strength of longitudinal specimens. The mechanical properties had previously been determined by Mr. Andrew (51) and their values are represented in Table 5. A cyclic maximum stress of 56 per cent of the ultimate tensile stress was usually sufficient to cause failure prior to 10^7 cycles. Test results were immediately plotted on an S-N diagram. Tests for which the specimen fractured are plotted as closed circles. A test which did not fail is plotted as a closed circle with an arrow.

The first test result was analyzed to choose a second test stress level estimated to be below the fatigue limit. If this choice was correct, the test was stopped after 10^7 cycles. An unbroken test specimen was frequently retested at a much higher stress level. The duplicate tests for a single specimen are connected with dashed lined on the S-N diagram. The result of each test was thus analyzed to establish the next test stress level. "No-failure" was defined for any test which ran 10^7 cycles or more without fracture. The fatigue limit was defined for each steel condition as the highest stress level at, or below which, no specimen failed.

Once the data was plotted for all test specimens in each

fabrication condition, a smooth curve was judiciously drawn among the data points in the high-stress, low-cycle region. A bend, or "knee," was drawn among those data points in the finite live region just above the fatigue limit. This knee connected the smooth curve with the horizontal line representing the determined fatigue limit. S-N curves for all fabrication conditions were drawn and presented as Figures 26 through 35.

Graphs were plotted to reveal possible relationships between the determined fatigue limits versus ultimate tensile strength, yield strength, hardness and grain size. The yield strength values were for the lower yield strength, with the exception of the samples fabricated at 800 and 950°F. These did not exhibit discontinuous yielding when tested in tension (51); therefore, the 0.2 per cent offset yield strength values were used. The hardness values were the results of Brinell hardness tests involving the application of 3,000 kg loads to 10 mm diameter spherical indentors. The grain size value used is better referred to as the ferrite mean intercept length (51).

Predicted fatigue limit values were computed using equation (1.3). This empirical equation was formulated by Rowe (44) and is an attempt to quantitatively calculate the fatigue limit for a probability of failure of 0.5 in terms of strength and work hardening. The values of the strain hardening exponent, n, and the strength coefficient, K, were average values determined by the method of Considieré's second finding for two longitudinal tensile test specimens per fabrication condition (51).

CHAPTER IV

RESULTS

The determined fatigue limits and computed fatigue ratios are presented in Table 3. Complete results of the fatigue testing program are given in Table 4. Predicted fatigue limits, as computed by Rowe's empirical formula, are tabulated in Table 5.

Results previously determined in a related investigation of this production heat of X-60-W steel are presented in the Appendices for their value in the interpretation of fatigue results. Table 6 is a tabulation of the previously determined mechanical properties. Table 7 presents the results of the optical metallographic investigation.

Table 3. Determined Fatigue Limits

Code	Fabrication Temperature ($^{\circ}$F)	Fatigue Limit (psi)	Fatigue Ratio
1	Mill	48,608	0.537
12	800	66,949	0.488
13	950	64,317	0.531
14	1100	59,541	0.554
15	1250	55,101	0.565
16	1400	47,161	0.519
17	1550	46,370	0.530
18	1700	45,292	0.528
19	1850	48,134	0.561
20	2000	45,765	0.517

Table 4. Fatigue Test Results.

Code	Finishing Temp. (°F)	Load (lbs)	Stress Amplitude (psi)	Percent UTS (%)	Cycles to Failure ($X\ 10^{-3}$)	Average Minimum Diameter (in)	Diameter Deviation (in)	Percent Out of Round (%)
1a	Mill	10.26	48,608	53.7	10419*	0.1631	0.0001	0.1
"	Mill	10.96	51,924	57.4	453	"	"	"
1b	Mill	10.36	49,082	54.3	1545	0.1625	0.0007	0.4
1c	Mill	10.56	51,221	56.6	1288	0.1619	0.0005	0.3
1d	Mill	10.26	47,503	52.5	14853*	0.1634	0.0007	0.4
"	Mill	10.76	49,818	55.1	1408	"	"	"
1e	Mill	10.16	49,280	54.5	1828	0.1618	0.0009	0.6
1f	Mill	10.46	49,556	54.7	2490	0.1627	0.0006	0.4
1h	Mill	11.96	56,662	62.6	138	0.1625	0.0011	0.7
12a	800	14.46	68,506	49.9	2829	0.1624	0.0008	0.5
12b	800	15.66	72,505	52.8	2786	0.1641	0.0004	0.2
12c	800	17.36	75,240	54.8	652	0.1677	0.0004	0.2
12e	800	15.26	74,018	53.9	675	0.1610	0.0000	0.0
12f	800	14.46	66,949	48.8	13848*	0.1644	0.0006	0.4
"	800	19.36	89,636	65.3	99	"	"	"
12g	800	16.86	81,778	59.6	334	0.1612	0.0000	0.0
12h	800	15.76	71,347	52.0	2831	0.1655	0.0006	0.4

* Indicates specimen had not failed

Table 4. Fatigue Test Results (Continued).

Code	Finishing Temp. (°F)	Load (lbs)	Stress Amplitude (psi)	Percent UTS (%)	Cycles to Failure ($X\ 10^{-3}$)	Average Minimum Diameter (in)	Diameter Deviation (in)	Percent Out of Round (%)
13a	950	13.66	64,716	53.4	3989	0.1627	0.0016	1.0
13b	950	14.36	66,486	54.9	4016	0.1641	0.0009	0.5
13c	950	13.46	65,287	53.9	3124	0.1609	0.0004	0.2
13e	950	13.56	64,242	53.0	11719*	0.1632	0.0008	0.5
"	950	16.16	76,560	63.2	486	"	"	"
13f	950	14.86	68,801	56.8	1407	0.1642	0.0019	1.2
13i	950	13.26	64,317	53.1	16577*	0.1616	0.0012	0.7
13j	950	16.56	78,455	64.8	311	0.1621	0.0018	1.1
14a	1100	12.56	60,921	56.7	3759	0.1612	0.0012	0.7
14b	1100	14.76	65,367	60.8	952	0.1661	0.0008	0.5
14c	1100	13.26	60,029	55.8	8462	0.1650	0.0011	0.7
14f	1100	12.86	59,541	55.4	18011*	0.1639	0.0006	0.4
14g	1100	14.86	70,401	65.5	418	0.1630	0.0020	1.2
14h	1100	13.36	59,167	55.0	14426*	0.1666	0.0020	1.2
"	1100	15.36	68,024	63.3	446	"	"	"
14i	1100	15.36	72,770	67.7	337	0.1624	0.0011	0.7

* Indicates specimen had not failed

Table 4. Fatigue Test Results (Continued).

Code	Finishing Temp. (°F)	Load (lbs)	Stress Amplitude (psi)	Percent UTS (%)	Cycles to Failure ($X\ 10^{-3}$)	Average Minimum Diameter (in)	Diameter Deviation (in)	Percent Out of Round (%)
15a	1250	13.36	63,295	64.9	584	0.1629	0.0007	0.4
15c	1250	11.26	55,948	57.4	6607	0.1606	0.0009	0.6
15d	1250	11.36	55,101	56.7	13258*	0.1617	0.0007	0.4
15e	1250	11.56	54,767	56.2	15330*	0.1629	0.0007	0.4
"	1250	13.76	65,190	66.8	373	"	"	"
15f	1250	11.86	60,402	61.9	1234	0.1591	0.0008	0.5
15i	1250	10.36	51,476	52.8	15006*	0.1600	0.0006	0.4
"	1250	11.76	58,432	59.9	16510*	"	"	"
"	1250	13.76	68,370	70.1	85	"	"	"
16b	1400	9.46	47,004	51.7	15467*	0.1596	0.0020	1.3
16c	1400	9.06	55,930	61.5	74	0.1495	0.0021	1.4
16d	1400	9.86	47,825	52.6	1053	0.1614	0.0016	1.0
16e	1400	9.26	47,161	51.9	15441*	0.1583	0.0024	1.5
16f	1400	11.46	48,638	53.5	1061	0.1688	0.0003	0.2
16g	1400	11.86	52,524	57.8	90	0.1662	0.0007	0.4
16h	1400	11.46	49,673	54.7	600	0.1673	0.0005	0.3
16i	1400	13.56	58,775	64.7	46	0.1675	0.0008	0.5

*Indicates specimen had not failed

Table 4. Fatigue Test Results (Continued).

Code	Finishing Temp. (°F)	Load (lbs)	Stress Amplitude (psi)	Percent UTS (%)	Cycles to Failure ($X\ 10^{-3}$)	Average Minimum Diameter (in)	Diameter Deviation (in)	Percent Out of Round (%)
17a	1550	9.86	46,713	53.3	1204	0.1624	0.0005	0.3
17b	1550	10.06	48,795	55.7	636	0.1619	0.0020	1.2
17c	1550	10.26	48,608	55.5	701	0.1632	0.0007	0.4
17d	1550	10.26	49,765	56.8	429	0.1610	0.0014	0.9
17e	1550	9.96	59,677	68.2	43	0.1508	0.0018	1.2
17f	1550	9.56	46,370	53.0	12179*	0.1610	0.0006	0.4
17g	1550	10.66	46,205	52.8	10866*	0.1673	0.0001	0.1
17h	1550	11.46	51,880	59.3	90	0.1645	0.0006	0.4
17j	1550	10.16	44,038	50.3	16850	0.1678	0.0008	0.5
"	1550	12.86	55,741	63.7	58	"	"	"
18c	1700	9.16	51,835	60.4	62	0.1539	0.0007	0.5
18d	1700	7.96	45,044	52.5	17077*	0.1527	0.0006	0.4
"	1700	9.96	56,362	65.7	50	"	"	"
18e	1700	9.66	46,855	54.6	270	0.1611	0.0000	0.0
18f	1700	9.96	45,090	52.6	16000*	0.1648	0.0010	0.6
"	1700	11.46	51,880	60.5	120	"	"	"
18g	1700	10.16	45,995	53.6	421	0.1652	0.0006	0.4
18h	1700	10.46	47,353	55.2	580	0.1657	0.0003	0.2
18j	1700	9.56	45,292	52.8	13616*	0.1625	0.0008	0.5
"	1700	10.36	49,082	57.2	934	"	"	"

*Indicates specimen had not failed

Table 4. Fatigue Test Results (Continued).

Code	Finishing Temp. (°F)	Load (lbs)	Stress Amplitude (psi)	Percent UTS (%)	Cycles to Failure ($X\ 10^{-3}$)	Average Minimum Diameter (in)	Diameter Deviation (in)	Percent Out of Round (%)
19a	1850	10.06	47,661	55.6	10472*	0.1626	0.0000	0.0
"	1850	11.36	53,819	62.8	273	"	"	"
19b	1850	10.16	48,134	56.1	18334*	0.1630	0.0008	0.5
19c	1850	9.96	47,187	55.0	14136*	0.1626	0.0014	0.9
"	1850	11.96	56,662	66.1	69	"	"	"
19e	1850	10.96	55,819	65.1	67	0.1581	0.0013	0.8
19f	1850	10.26	48,608	56.7	1209	0.1629	0.0006	0.4
19g	1850	11.16	50,522	58.9	126	0.1645	0.0015	0.9
19i	1850	10.06	48,795	56.9	427	0.1618	0.0024	1.5
20a	2000	9.56	46,370	52.4	3040	0.1609	0.0009	0.6
20b	2000	9.36	45,400	51.3	18377*	0.1611	0.0004	0.2
"	2000	10.96	53,160	60.0	107	"	"	"
20d	2000	9.66	45,765	51.7	15237*	0.1630	0.0004	0.2
"	2000	11.26	53,346	60.3	254	"	"	"
20h	2000	12.76	59,078	66.7	47	0.1636	0.0017	1.0
20i	2000	10.26	48,608	54.9	1199	0.1628	0.0002	0.1
20j	2000	10.16	45,995	52.0	1529	0.1645	0.0008	0.5

* Indicates specimen had not failed

Table 5. Predicted Fatigue Limits for a Probability of Failure of 0.5.

Code	Fabrication Temp.	Strain Hardening Exponent	Strength Coefficient	Predicted Fatigue Limit*
		n	K	
	(°F)		(psi)	(psi)
1	Mill	0.1311	134,570	52,261
12	800	0.0397	162,340	79,016
13	950	0.0578	151,355	66,480
14	1100	0.0811	142,980	58,935
15	1250	0.0931	133,515	54,168
16	1400	0.1151	130,750	51,661
17	1550	0.1643	138,825	52,635
18	1700	0.1389	129,642	50,220
19	1850	0.1428	130,555	50,405
20	2000	0.1350	132,740	51,458

* Computed by Rowe's empirical formula (43).

CHAPTER V

DISCUSSION

General

Examination of Figures 7 and 8 reveals that the test data for all fabrication conditions falls into two categories.

Fatigue test results for the mill condition steel, and the results for all tests on specimens fabricated at 1400°F or higher, fit into a relatively compact band in Figure 7. Analysis of Figure 8 reveals that the lowest determined fatigue limit, that for the 1700°F fabricated steel, is only 7 per cent less than that of the mill supplied material.

From knowledge of the statistical variability of fatigue data, it is conceivable that this compact band of fatigue test results could be duplicated by a large sample size test upon a single test population. Assume that testing of a hypothetical, homogeneous steel population resulted in a determined fatigue limit of 46,950 psi with a probability of failure of 0.5. If the standard deviation of the fatigue limit of this hypothetical steel was found to be 1,658 psi, then a range which included one standard deviation above and below the 0.5 probability level would include all determined fatigue limits of the narrow band of data under consideration. Ranson and Mehl have demonstrated that a standard deviation this large was found for longitudinal specimen tests of a 4340 steel (23). Therefore, with knowledge of the

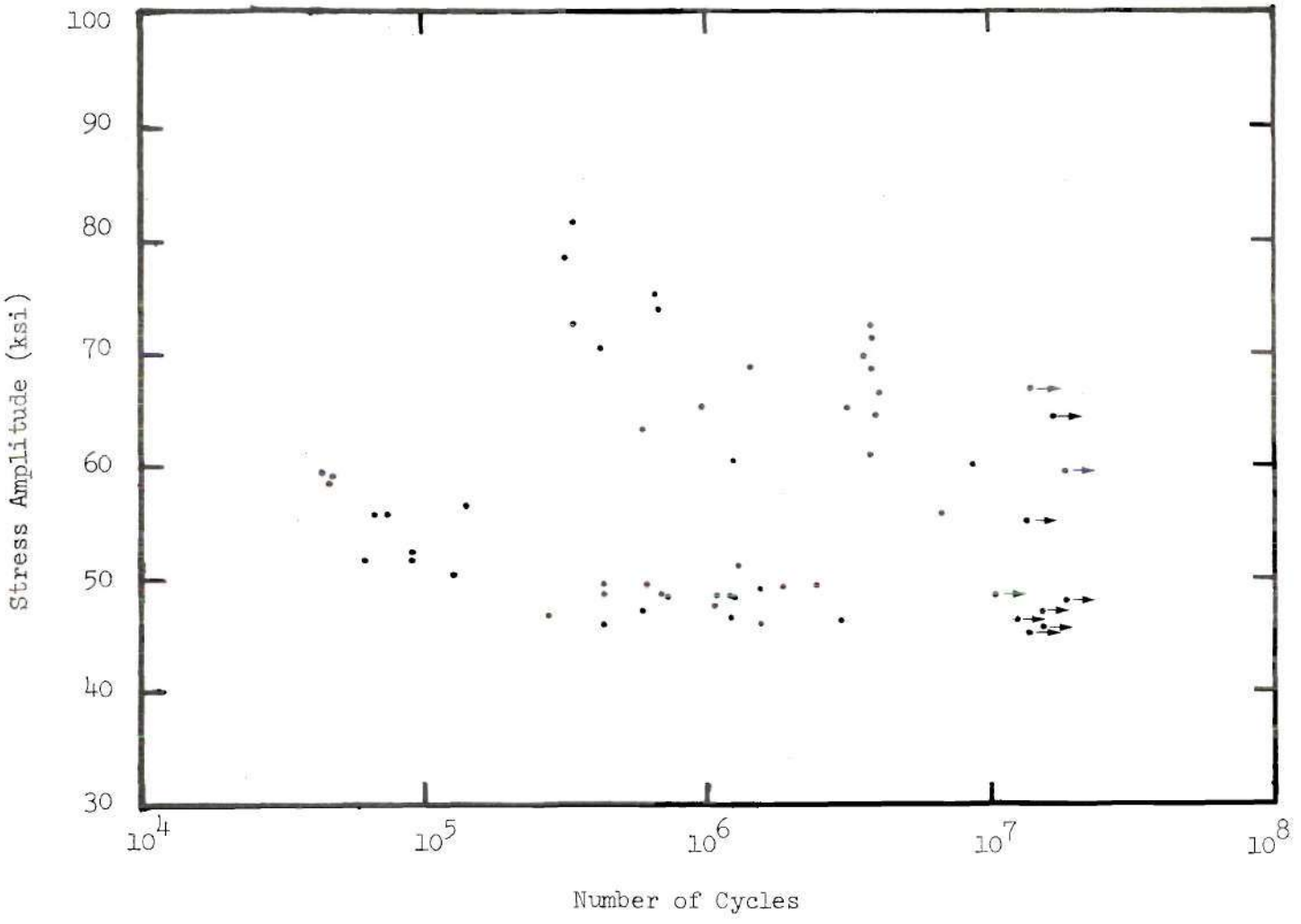

Figure 7. Fatigue Test Results for All Fabrication Conditions.

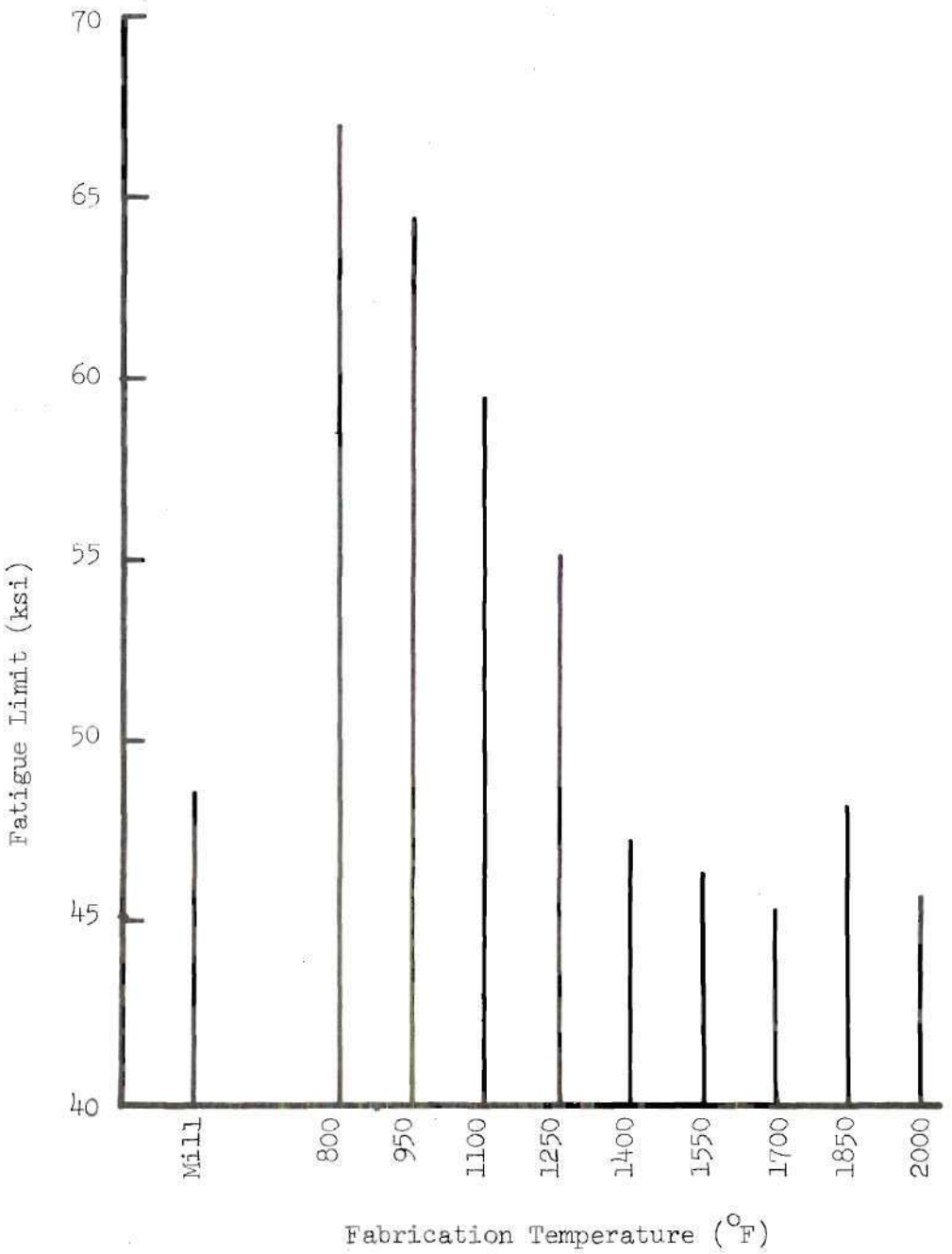

Figure 8. Comparison of Fatigue Limits.

small number of tests which determined the fatigue limits for the aforementioned fabrications conditions of X-60-W steel, a statistical conclusion that the plates which were fabricated above 1400°F possess true fatigue limits below that of the mill supplied material cannot be made. However, examination of Figures 7 and 8 reveals that the determined fatigue limits for all plates fabricated above 1400°F are less than that of the mill condition material. Apparently, the fatigue limit of X-60-W steel is decreased slightly by reheating and fabrication in the austenitic region.

Referring again to Figure 7 and 8, it is observed that the fatigue strengths of the 800 through 1250°F fabricated plates are considerably greater than those of the previous six mentioned fabrication conditions. If individual S-N curves are drawn on Figure 7 for each of these low temperature fabrication conditions, it will be observed that their S-N curves are similar; and that as the temperature of reheating and fabrication decreases in this range, fatigue strength rises. Analysis of Figure 8 reveals that the fatigue limit of 800°F fabricated plate is greatest, and that it is 46 per cent more than that of the mill supplied material.

Fatigue Limit Correlation With Property Parameters

Variations of the determined fatigue limits for the various fabrication temperatures were plotted on Cartesian coordinates against their corresponding values of hardness, static tensile strength, yield strength and grain size. Also, Rowe's method to predict the fatigue

limit based on the strain hardening exponent and strength coefficient was tested.

Correlation With Hardness

The Brinell hardness number (BHN) for each fabrication condition is plotted against the determined fatigue limit in Figure 9. Data regression analysis yield the indicated linear relationship between increasing hardness and increasing fatigue limit. The determined correlation coefficient of 0.9859 indicated excellent correlation between the BHN and fatigue limit for all test conditions.

Correlation With Static Tensile Strength

Figure 10 reveals the relationship of the fatigue limit to the ultimate tensile strength. Very good linear correlation was found as the correlation coefficient was calculated as 0.9629.

Correlation With Yield Strength

Very good correlation was also found for a linear relationship between increasing yield strength and a corresponding increasing fatigue limit. The correlation coefficient was 0.9587. This linear relationship is shown in Figure 11.

Correlation With Grain Size

Test condition fatigue limit values were plotted against the corresponding microstructural grain sizes (as determined by the ferrite mean intercept method) in Figure 12. This graph revealed no linear relationship between these two material properties. This is in agreement with general findings that for wrought ferritic steels, the fatigue limit is not a function of microstructural grain size (43).

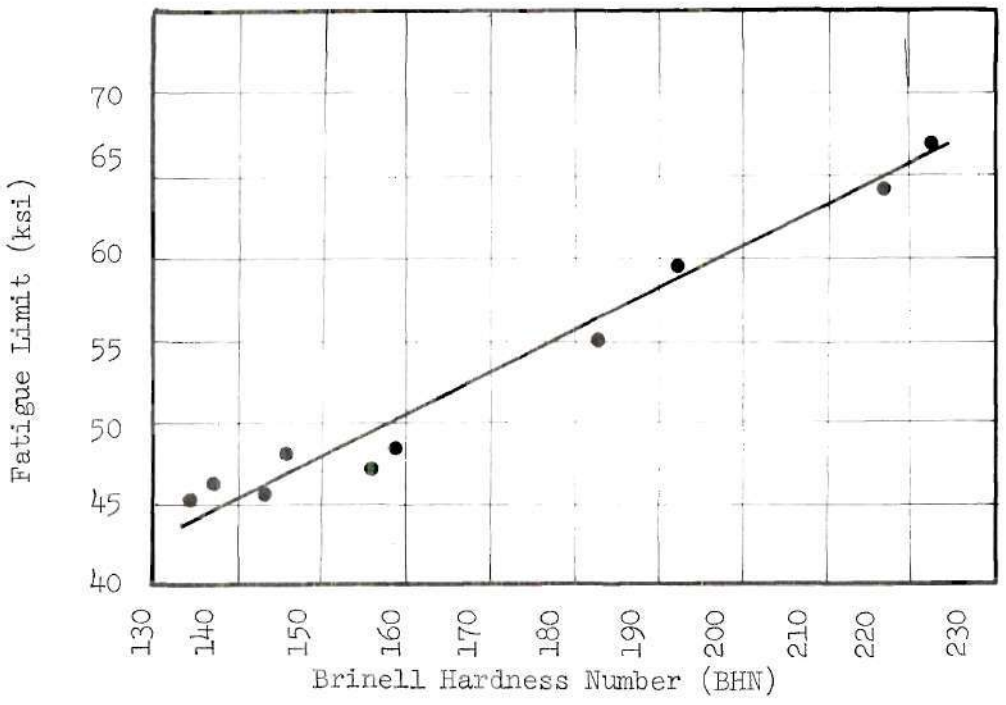

Figure 9. Fatigue Limit as a Function of Surface Hardness.

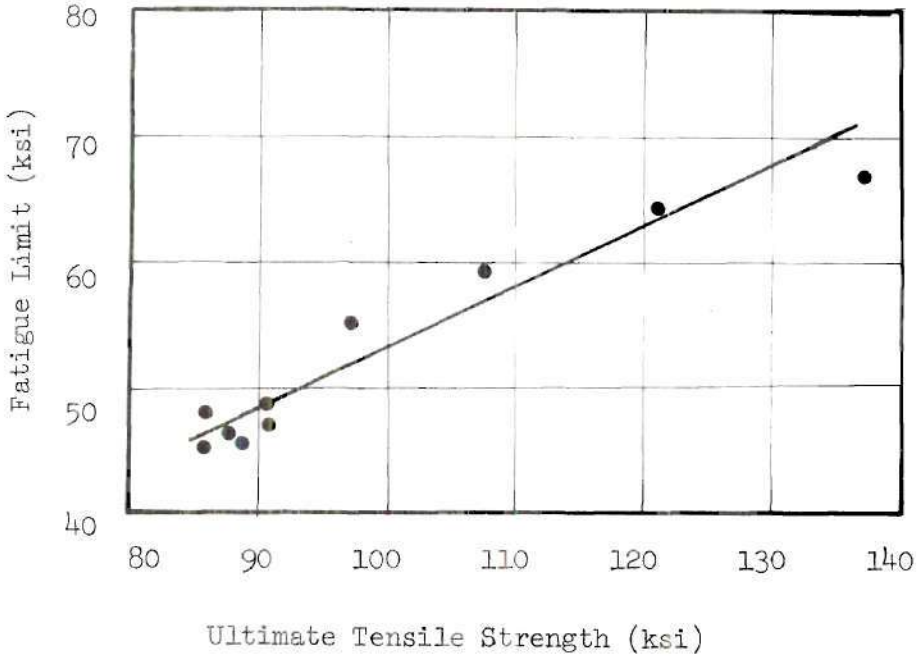

Figure 10. Fatigue Limit as a Function of Ultimate Tensile Strength.

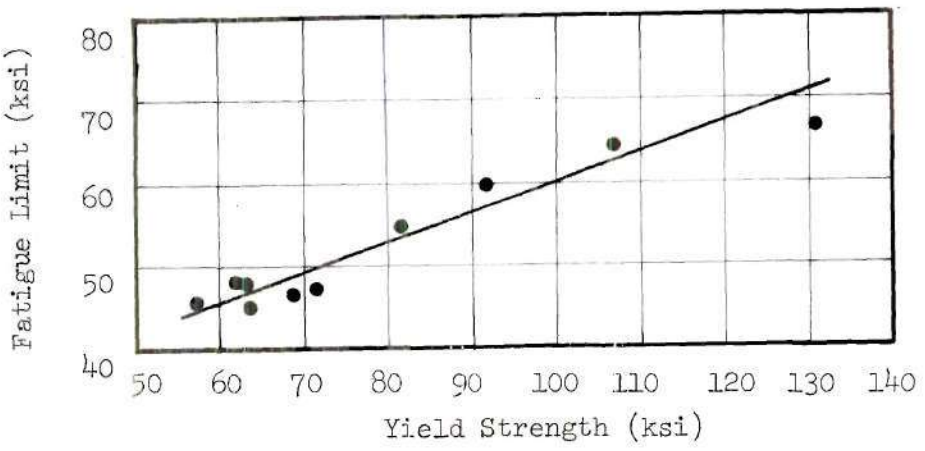

Figure 11. Fatigue Limit at a Function of Yield Strength

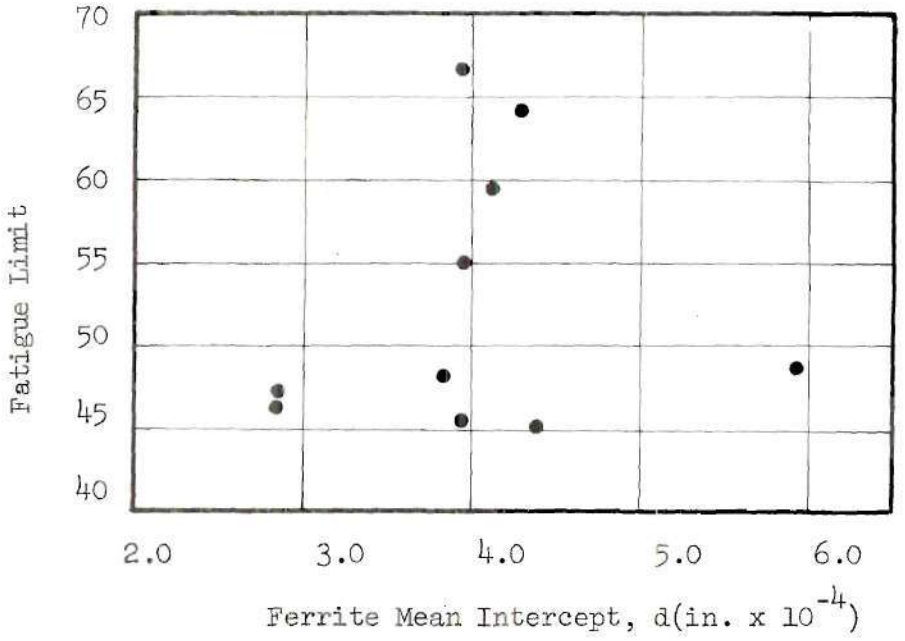

Figure 12. Fatigue Limit as a Function of Grain Size

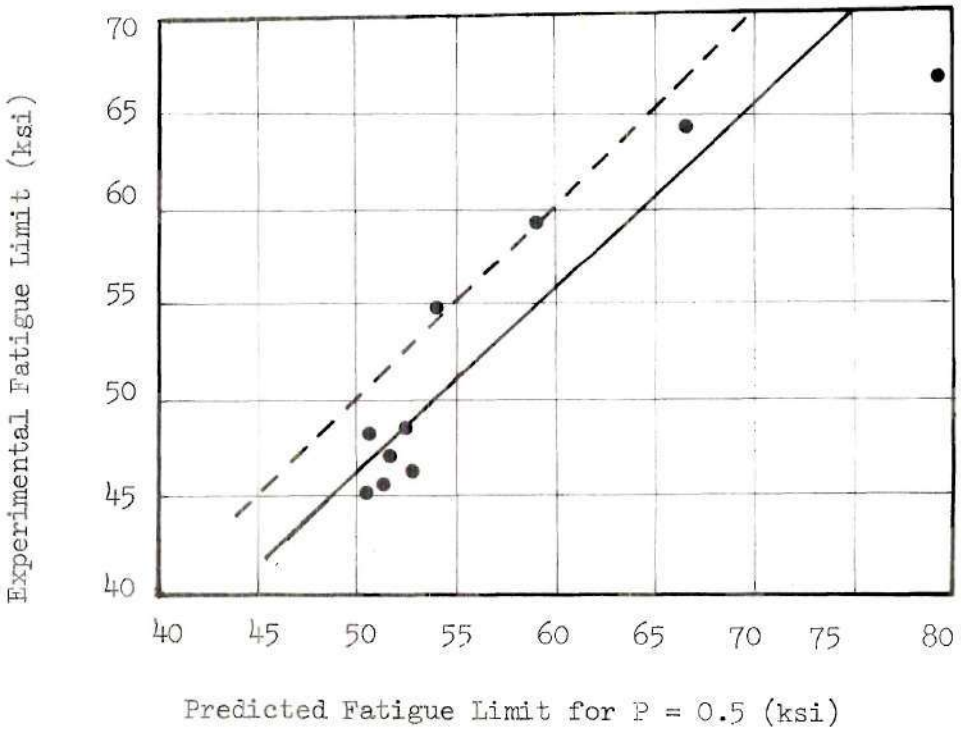

Figure 13. Relationship of the Experimental Fatigue Limit With Rowe's Equation.

Applicability of Rowe's Method to Predict the Fatigue Limit

Predicted fatigue limit values computed by Rowe's empirical formula were plotted against the experimental test values in Figure 13. The best linear relationship as determined by data regression analysis appears as a solid line of this graph. Good correlation of data about this line of best fit is evidenced by the determined correlation coefficient of 0.9157. A dashed line in Figure 13 represents ideal, one to one, correspondence between predicted and experimental values. It is significant that the experimental line of best fit lies below, and approximately parallel to the ideal line. Rowe's method predicts the true fatigue limit for a probability of failure of 0.5; whereas the experimental fatigue limit was simply the highest stress level below which failure was not experienced after ten million cycles for a small population size test. Therefore, it would be expected that predictions by Rowe's method would have higher values than the reported experimental results. In view of these qualifying considerations, it is felt that Rowe's method successfully predicts the fatigue limit of X-60-W steel.

The above five data correlation studies should now be considered in perspective. Good correlation was shown for the derived linear relationships of the BHN, static tensile strength and yield strength with the experimental fatigue limit values. However, it must be emphasized that the linear relationships observed are applicable only for X-60-W steel. If fatigue testing were performed on a steel of some other composition which was subjected to a similar series of

thermomechanical treatments, it would be expected that similar plots of these mechanical properties against the experimental determined fatigue limits would also yield good linear correlation. However, the slope and intercepts of these lines would not likely be identical to those determinable from this investigation.

On the other hand, Rowe's method apparently successfully predicts fatigue limit values for plain carbon and low alloy steels based upon parameters obtainable from a simple static tensile test.

Optical Photomicrographs

The microstructure of X-60-W steel as received in the mill supplied condition, after reheating and rolling at two temperatures which may be considered as warm-rolling, at two temperatures within the two-phase ferrite-austenite region, and at a temperature which was sufficiently high to be considered within the single phase austenite region are presented in this section of the text. Figures 15 and 16 are the microstructures resulting from fabrication at 950 and 1250^{o}F respectively. The work hardening effects are evident because of the elongated grain structures in the rolling directions. The steel fabricated at 1400^{o}F (Figure 17) reveals a mixed microstructure of partially recrystallized ferrite and elongated pearlite. This temperature was apparently close to the eutectoid temperature. It can be concluded that this microstructure is a result of an isoforming process. In Figure 18 the material was fabricated at 1550^{o}F. The austenite grains had little time for recovery after deformation and transformed to a very desirable microstructure of fine equiaxed ferrite and pearlite.

Figure 14. Optical Photomicrograph of the Mill Condition Steel, Magnification 400X.

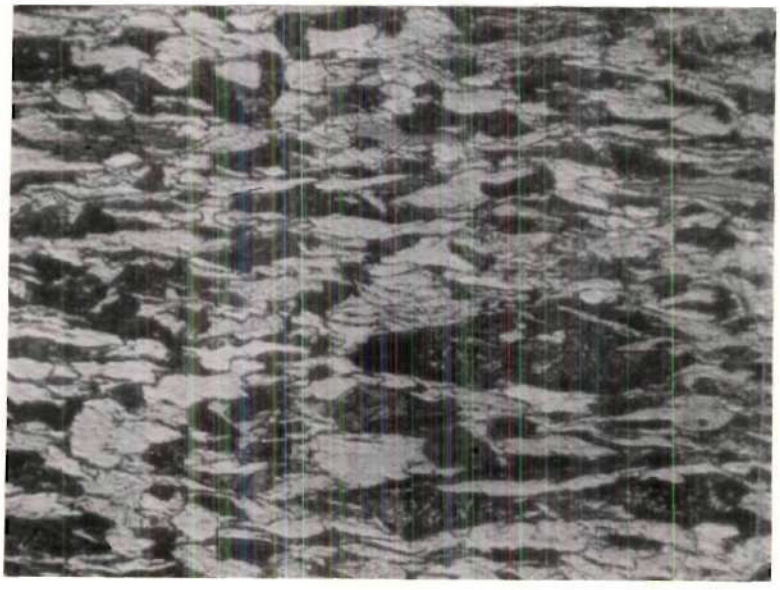

Figure 15. Optical Photomicrograph of the Steel Fabricated at 950°F, Magnification 400X.

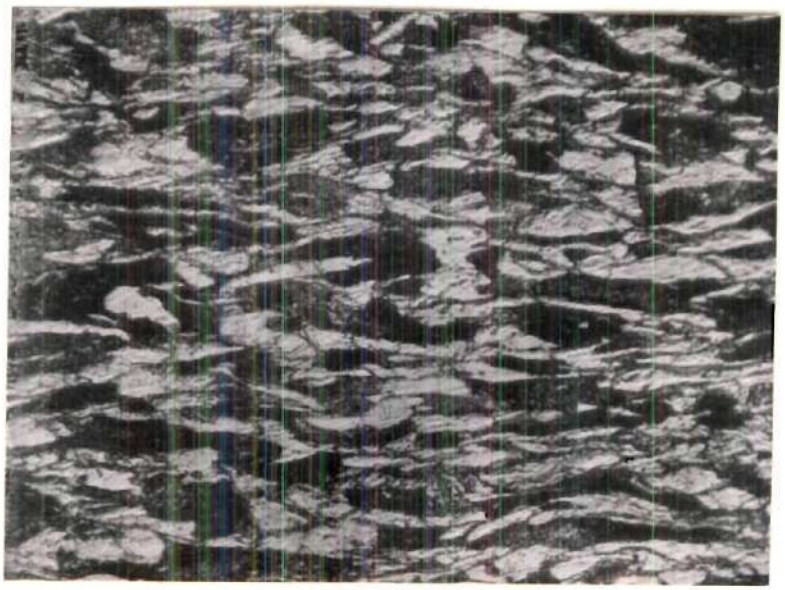

Figure 16. Optical Photomicrograph of the Steel Fabricated at 1250°F, Magnification 400X.

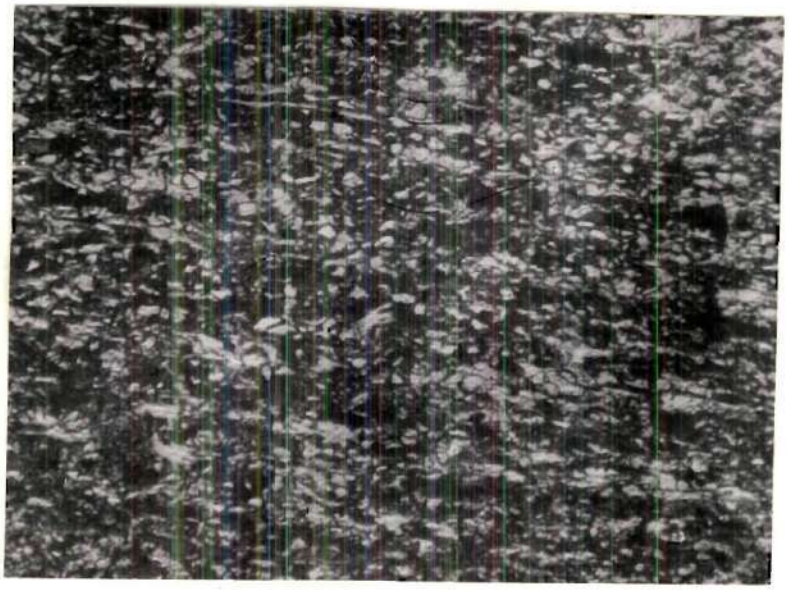

Figure 17. Optical Photomicrograph of the Steel Fabricated at 1400°F, Magnification 400X.

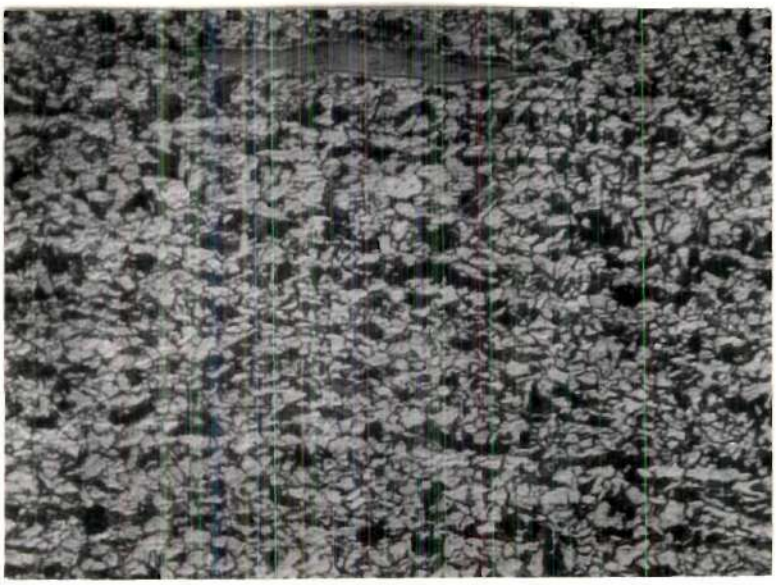

Figure 18. Optical Photomicrograph of the Steel Fabricated at 1550°F, Magnification 400X.

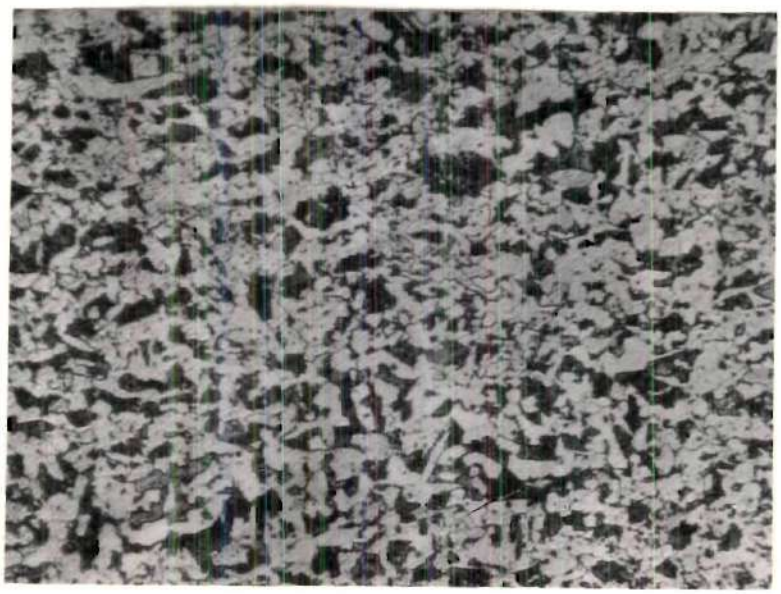

Figure 19. Optical Photomicrograph of the Steel Fabricated at 1700°F, Magnification 400X.

This microstructure is characteristic of good process control of rolling at low temperatures in the austenitic region. Figure 19 shows the microstructure fabricated at 1700°F. As this temperature was well within the single-phase austenitic region during the initial mill pass, austenitic recrystallization and grain growth was possible prior to transformation to ferrite thus resulting in a larger ferrite final grain size upon transformation.

Electron Photomicrographs

As a part of this investigation, the microstructural variations observable through transmission electron microscopy were studied. Of primary concern was the possible variation of matrix precipitates with varying fabrication temperatures. Electron photomicrographs of the mill condition steel and the steel plates which had been reheated and rolled at 950, 1250, 1550, and 1850°F are presented as Figures 20, 21, 22, 23 and 24. Observation of these micrographs revealed the presence of two size ranges of precipitates. Neither the range of diameters, nor the quantity of each size range appeared to vary among the various studied microstructures. A search of the published literature discovered two articles which contained electron photomicrographs of a mild steel of the following analyzed weight per cent composition: 0.26 C, 1.15 Mn and 0.03 Si (53,54). This steel was very similar in composition to Republic X-60-W steel with the exception that it lacked a columbium alloying addition. The precipitates revealed by Figures 20 through 24 were not observable in the electron photomicrographs of the non-columbium addition steel.

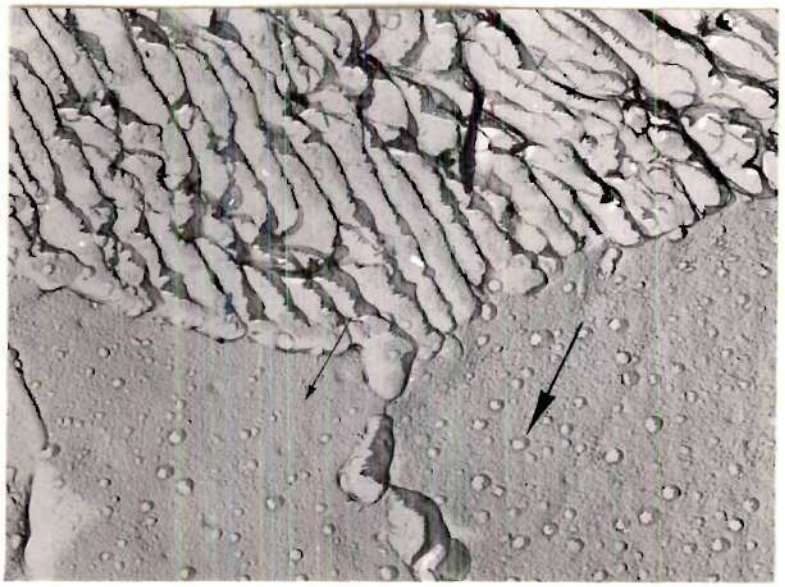

Figure 20. Electron Photomicrograph of the Mill Condition Steel, Magnification 12,000X.

Figure 21. Electron Photomicrograph of the Steel Fabricated at 950°F, Magnification 12,000X.

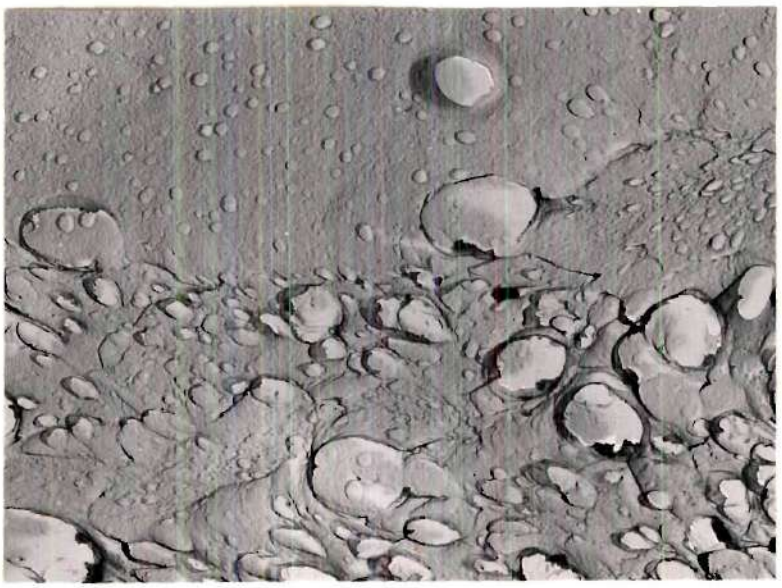

Figure 22. Electron Photomicrograph of the Steel Fabricated at 1250°F, Magnification 12,000X.

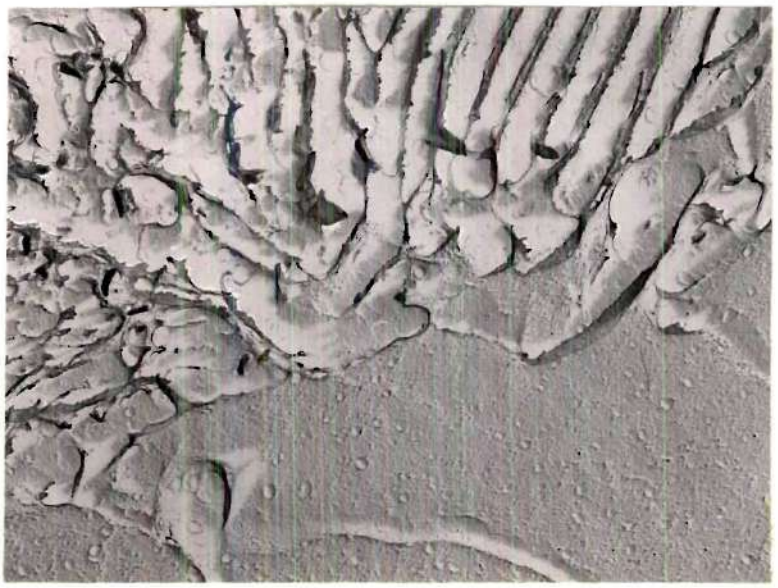

Figure 23. Electron Photomicrograph of the Steel Fabricated at 1550°F, Magnification 12,000X.

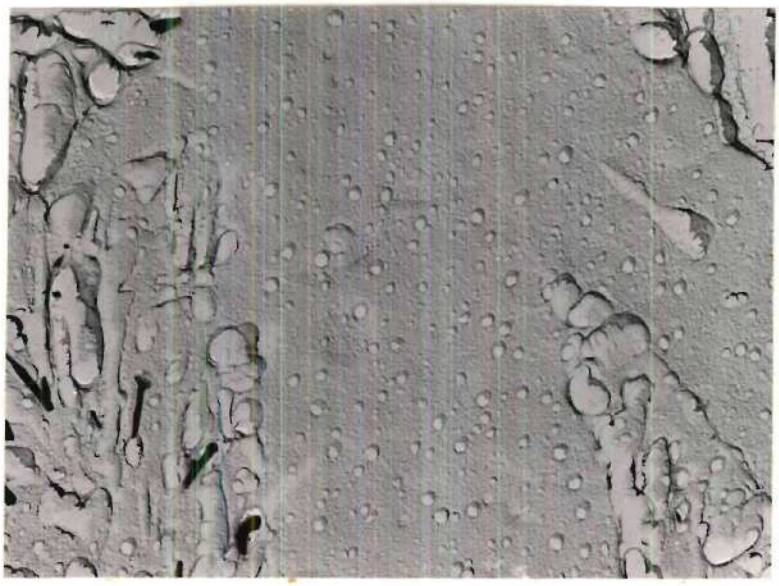

Figure 24. Electron Photomicrograph of the Steel Fabricated at 1850 F, Magnification 12,000X.

Based upon a consideration of the precipitation mechanisms known to exist for columbium carbides in steel, of the very stable nature of columbium carbides, and upon evidence that similar precipitates do not occur if columbium is absent, the conclusion was reached that the microstructures presented in this text revealed the following columbium carbide precipitates:

(1) Large CbC precipitates of 800 to 3000 Å diameter which were precipitated during commercial controlled rolling in the single phase austenitic region. Only a few are observed in Figure 23, however, adjacent ferrite grains had larger quantities of these particles. These large precipitates are denoted by large arrow on Figure 20.

(2) Very small CbC precipitates estimated to be greater than 50 Å. No definite "Row-pattern" is observable. It is believed that these precipitated at the austenite-ferrite interface during the commercial cooling and that these were the precipitates which most effectively retarded recrystallization and grain growth during subsequent reheating, rolling and cooling. These precipitates are indicated by a small arrow on Figure 20.

It was gratifying to receive substantiative comment from Dr. Davenport regarding these observable precipitates (55).

Explanations for Fatigue Strength Variations With Changes in the Fabrication Temperature

Specimens reheated and rolled at temperatures of 800, 950, 1100, and 1250°F demonstrated gradually increasing fatigue limits with decreasing fabrication temperature. The plate rolled at 800°F demon-

strated the greatest increase of 46 per cent as compared with the mill supplied steel. These fatigue strength increases are directly related to the ability of the steel to resist slip after cooling to room temperature. The ferrite grains of the steel rolled at 800°F would have less time to undergo recovery from the strain hardening effects of rolling as compared with that steel rolled at 1250°F. Columbium carbides were unaltered by these fabrication schedules. The stability of columbium carbides is so great that columbium addition steels will not suffer an appreciable decrease of hardness even when held for up to 100 hours at 700°C (1292°F) (13). The extremely small CbC precipitates effectively pinned the dislocation tangles in ferrite created by warm-rolling and thus retarded recovery during cooling to room temperature. The strong, slip-resistant grains produced by warm-rolling resulted in higher fatigue properties of these specimens as compared with the mill condition steel.

The plates reheated and rolled at 1400°F and above all exhibited fatigue limits below that of the mill condition steel. The greatest decrease of 7 per cent occurred for the 1700°F plate. The fatigue limits progressively decreased with increasing temperature from 1400 to 1700°F. Then, at 1850°F, the fatigue limit had risen to a value only 1 per cent less than that of the mill supplied steel. However, a decrease was again noted for the 2000°F rolled plate which had a fatigue limit only slightly higher than the minimum observed.

The following explanations are offered for the decreased fatigue strength of steel plates rolled at temperatures above 1400°F.

It is known that columbium addition steels suffer an almost instantaneous loss of hardness when the ferrite transofrms to austenite upon heating. This loss of matrix strength is associated with the relief of coherency stresses associated with the very small CbC precipitate in the ferrite matrix. The size range of the coherent precipitate of 20 to 50 Å. Therefore, it is difficult to resolve even through the application of electron microscopic techniques. Upon transformation of the matrix to austenite, this extremely small coherent precipitate acts as the nucleus for the growth of a stable incoherent particle which is effective for grain growth restriction, yet no longer effective to influence the frictional stress (12).

The above precipitation change mechanism can explain the observed fatigue limit drop. The steel heated and rolled at 1400°F was only slightly above its eutectoid temperature, thus it was in the two-phase region where both ferrite and austenite were stable. The percentage of ferrite remaining at any temperature within this two-phase region would be governed by the well known lever rule. The coherent precipitates present in the untransformed ferrite grains would retain their strengthening ability upon recooling of the steel to room temperature. Thus the ability of the matrix to resist slip, as governed by the quantity of coherent precipitates present, would progressively decrease as less and less ferrite was stable at each higher reheating temperature above 1400°F. A minimum for the fatigue limit was observed at the 1700°F rolling temperature where only austenite would be stable as this temperature is sufficiently high

to be considered well above the A_3 line of the metastable iron-carbon phase diagram.

Above 1000°C (1832°F), smaller columbium carbides can enter solid solution in austenite (16). Therefore, some dissolving of the smallest precipitates would be expected at the 1850 and 2000°F heating and rolling temperatures. The columbium taken into solid solution at these high temperatures could reprecipitate in the ferrite upon cooling as the extremely small, coherent columbium carbide which effectively strengthens the ferrite. It is notable, however, that the plates rolled at 1850 and 2000°F both exhibited experimental fatigue limits below that of the mill condition steel.

In closing, the idea that an engineering designer must consider fatigue strength as only one of many important material properties must be reemphasized. The results of this investigation must be considered in light of the previous investigation which established the material properties determinable through tensile, impact and surface hardness testing (51). Toughness of a steel, i. e., its resistance to the occurrence of brittle fracture, is perhaps the most important material property. Reference to Table 6 reveals that a greatly decreased 15 ft-lb Charpy V-notch transition temperature was found for reheating and rolling at 1550°F. It is therefore concluded that rolling at 1550°F resulted in the optimum combination of mechanical properties for X-60-W steel.

CHAPTER VI

CONCLUSIONS

1. Substantial increases in the fatigue strength of X-60-W steel were obtained by warm-rolling at temperatures of 1250°F or less.

2. The fatigue strength decreased slightly when X-60-W steel was reheated and rolled at temperatures of 1400°F or more.

3. Good linear correlation was demonstrated between the fatigue limit and the surface hardness, the ultimate tensile strength, and the yield strength.

4. Rowe's empirical equation satisfactorily predicted the fatigue limit behavior of X-60-W steel with variations in fabrication temperature.

5. It is concluded that, if toughness is considered the most important material design property, then the fine grained structure obtained by reheating and rolling at 1550°F resulted in the optimum set of material properties of X-60-W steel as compared with the mill supplied steel.

APPENDIX A

CALCULATION OF APPLIED STRESS

The stress experienced by a specimen is computed by the flexural formula for pure bending of a simple beam as shown in Figure 25.

$$S_s = \frac{-M_z y}{I_{zz}}$$

where: S_s = shear stress at a point

M_z = bending moment

I_{zz} = second moment of inertia about the neutral axis

y = distance from the neutral axis

The bending moment at either end is given by:

$$M_z = \frac{1}{2} WL$$

where: W = total effective load

L = moment arm length (4 in.)

The maximum tensile stress will occur within the gage section, at the minimum diameter, and at the bottom surface.

$$S_{max} = \frac{16WL}{\pi D^3}$$

where: D = specimen minimum diameter.

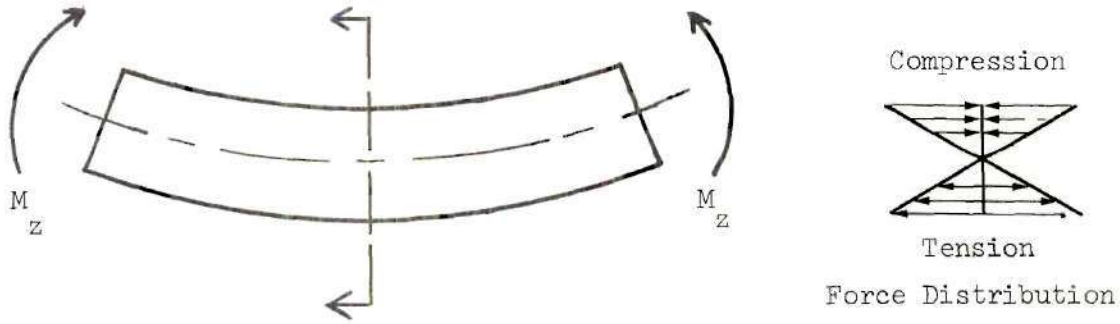

Figure 25. Simple Beam in Bending.

APPENDIX B

PREVIOUSLY DETERMINED PROPERTIES OF REPUBLIC X-60-W STEEL, HEAT # 41588

Table 6. Mechanical Properties, Average Values for Longitudinal Specimens

Fabrication Temp. (°F)	Ultimate Tensile Strength (psi)	Lower Yield Strength (psi)	15 Ft-Lb Charpy V-Notch Transition Temp. (°F)	Brinell Hardness Number (BHN)
Mill	90,450	61,815	+9	159
800	137,265	131,120*	+129	223
950	121,165	106,825*	+78	217
1100	107,535	91,915	+30	192
1250	97,535	81,295	+8	183
1400	90,875	71,235	-52	156
1550	87,560	68,305	-122	137
1700	85,770	63,495	-108	134
1850	85,730	62,885	+34	146
2000	88,530	57,600	+6	143

* Indicates 0.2 percent offset yield strength

Table 7. Optical Metallographic Results

Fabrication Temp. (°F)	Magnification	Ferrite Mean Intercept (in X 10^{-4})	Pearlite Volume Percent (%)	Ferrite Orientation Factor (%)
Mill	400X	5.93	45	8.27
800	400X	3.94	50	47.14
950	400X	4.29	45	56.01
1100	400X	4.10	56	53.50
1250	400X	3.94	52	56.80
1400	400X	2.83	45	45.10
1550	400X	2.82	36	14.80
1700	400X	4.40	42	29.30
1850	400X	3.82	43	9.30
2000	400X	3.95	49	19.00

APPENDIX C

S-N DIAGRAMS FOR ALL FABRICATION CONDITIONS

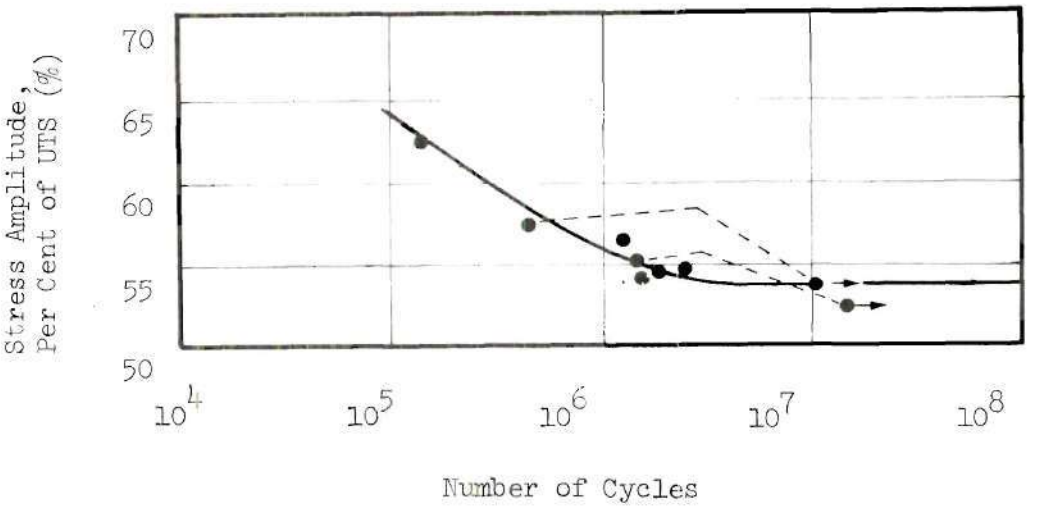

Figure 26. S-N Diagram for Mill Condition Steel.

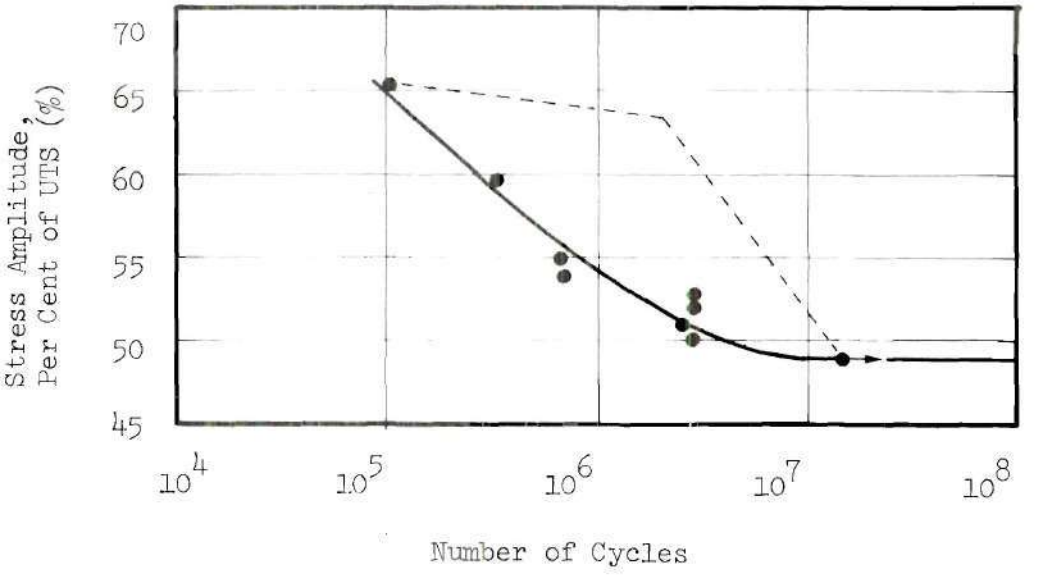

Figure 27. S-N Diagram for Steel Rolled at 800°F.

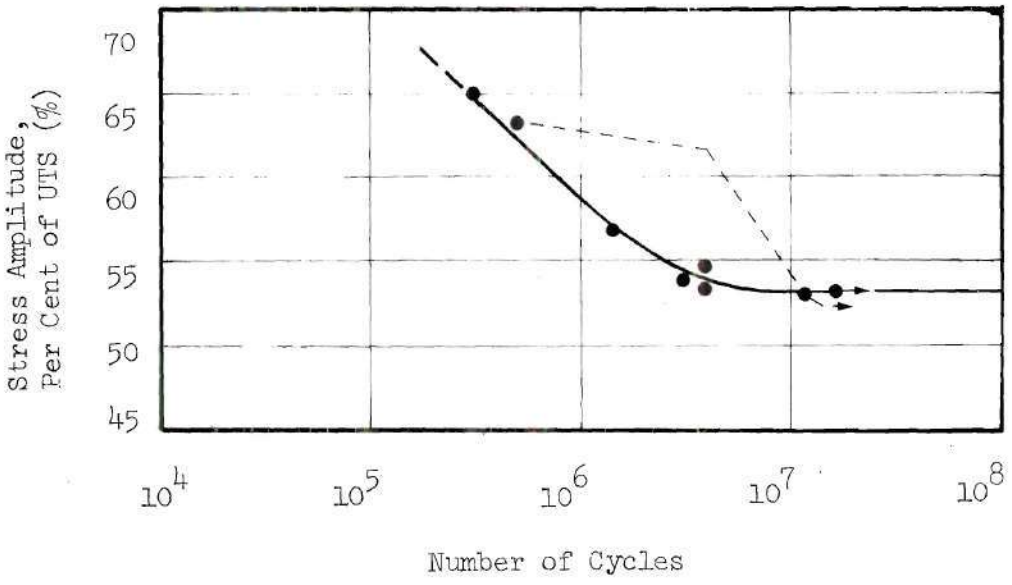

Figure 28. S-N Diagram for Steel Rolled at 950°F.

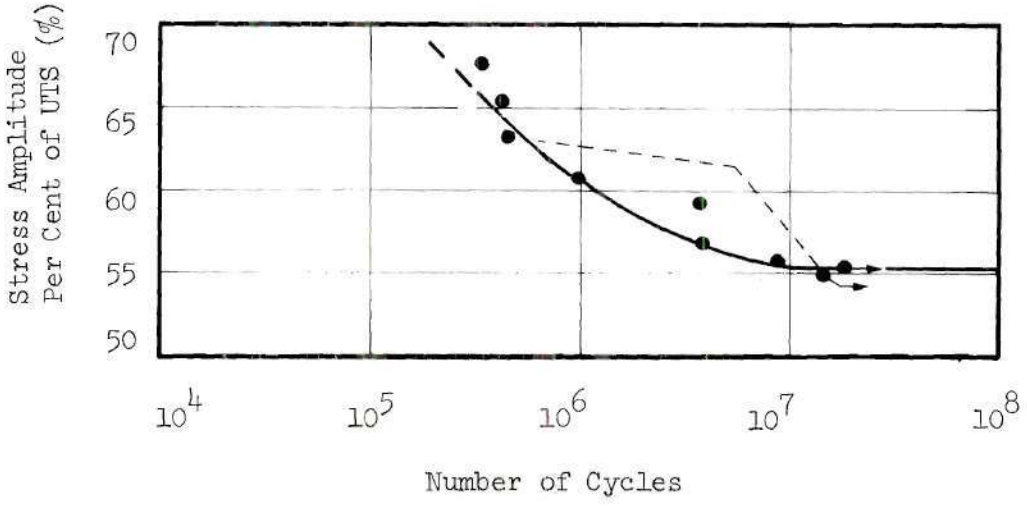

Figure 29. S-N Diagram for Steel Rolled at 1100°F.

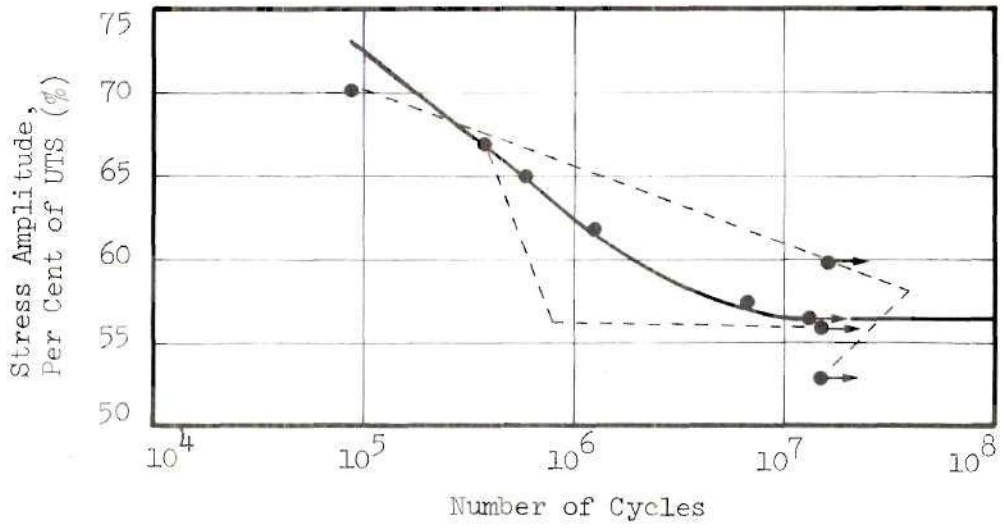

Figure 30. S-N Diagram for Steel Rolled at 1250°F.

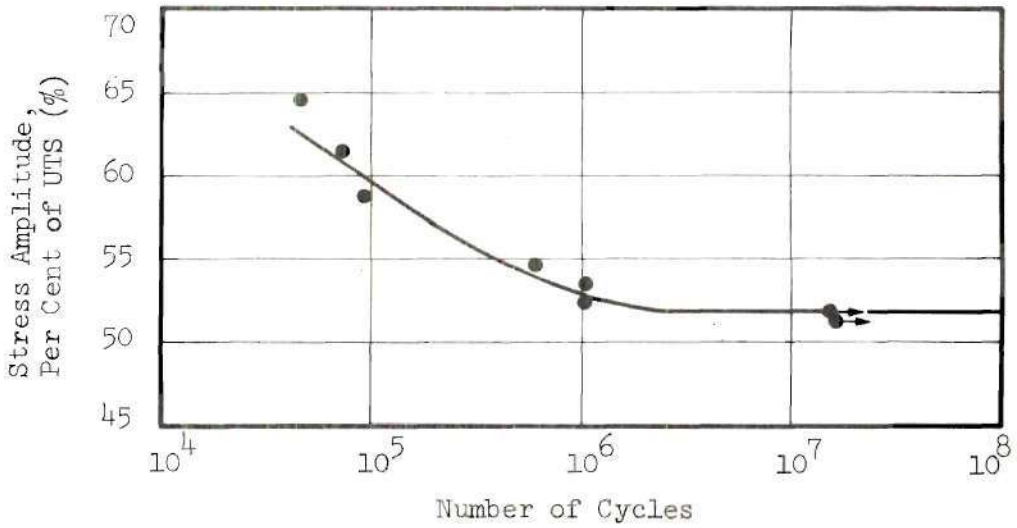

Figure 31. S-N Diagram for Steel Rolled at 1400°F.

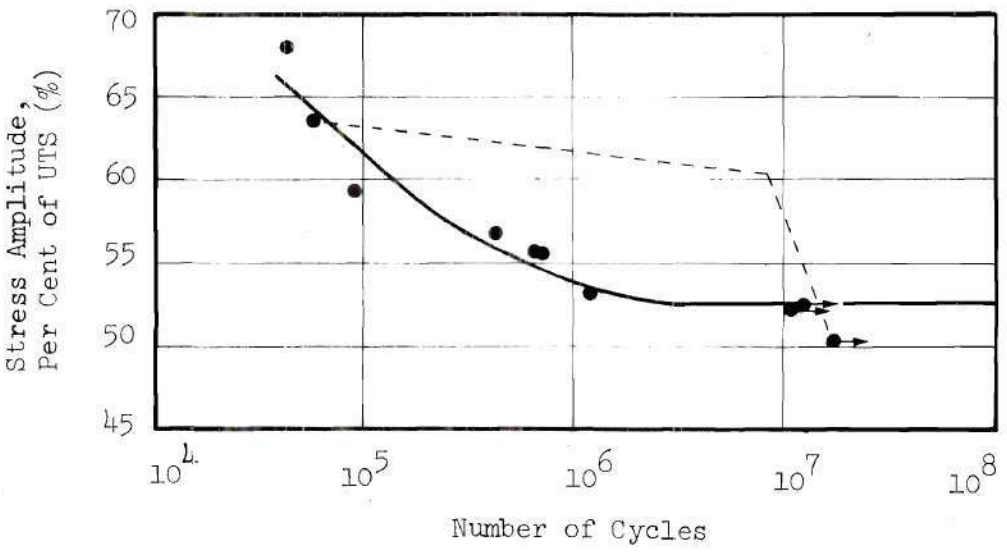

Figure 32. S-N Diagram for Steel Rolled at 1550°F

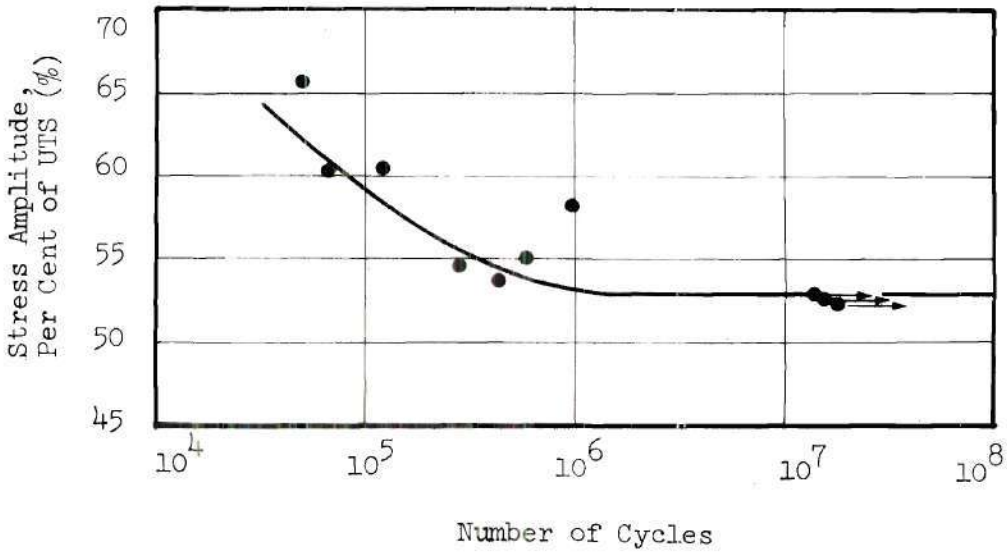

Figure 33. S-N Diagram for Steel Rolled at 1700°F

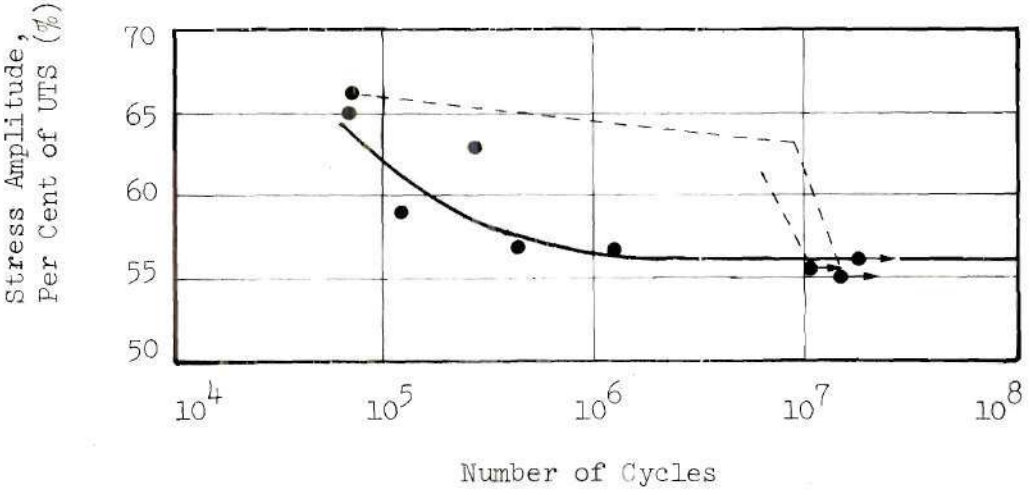

Figure 34. S-N Diagram for Steel Rolled at 1850°F.

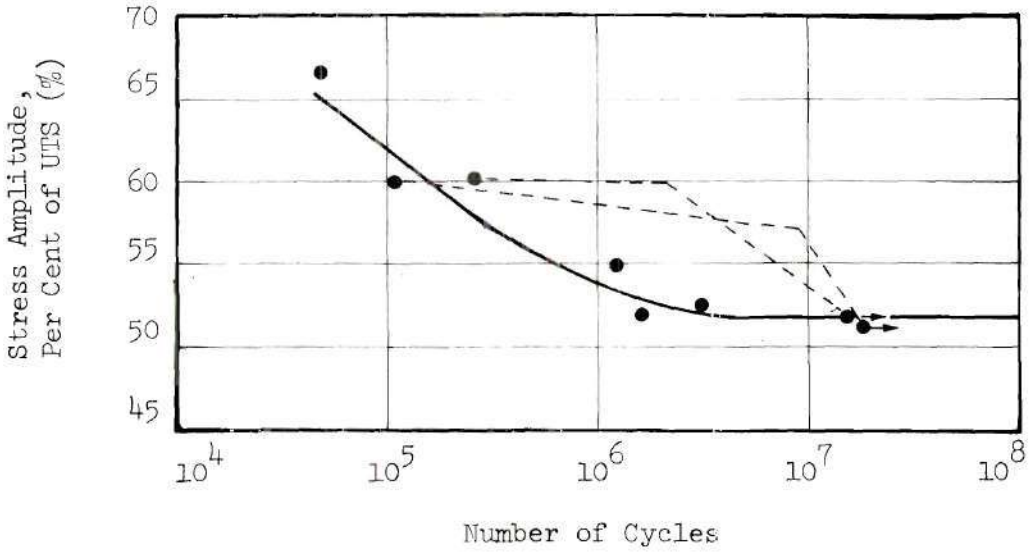

Figure 35. S-N Diagram for Steel Rooled at 2000°F.

BIBLIOGRAPHY

1. H. E. McGannon, ed., The Making, Shaping and Treating of Steel, 8th ed., pp. 716-723, United States Steel Corporation, Pittsburgh, Pennsylvania, 1964.

2. J. E. Shigley, Mechanical Engineering Design, 2nd ed., p. 247, McGraw-Hill Book Company, New York, 1972.

3. A 572-70a, 1972 Annual Book of ASTM Standards, Part 4, American Society for Testing and Materials, pp. 684-689.

4. McGannon, pp. 1098-1103.

5. K. Winterton, "Weldability Prediction from Steel Composition to Avoid Heat-Affected Zone Cracking, " The Welding Journal, 1961, Vol. 40, Research Supplement, pp. 253-s to 258-s.

6. R. B. G. Yeo, A. G. Melville, P. E. Repas, J. M. Gray, "Properties and Control of Hot-Rolled Steels," Journal of Metals, 1968, Vol. 20, No. 6, pp. 33-43.

7. W. J. Murphy and R. B. G. Yeo, "Developments in Plate and Structural High-Strength Steels," Metal Progress, 1969, Vol. 96, No. 3, pp. 85-89.

8. F. B. Pickering and T. Gladman, "An Investigation Into Some Factors Which Control the Strength of Carbon Steels," Iron and Steel Institute Publication 81, 1963, pp. 10-20.

9. W. E. Duckworth, "Metallurgy of Structural Steels: Present and Future Possibilities," ISI Publication 104, 1967, pp. 61-73.

10. D. S. Clark and W. R. Varney, Physical Metallurgy for Engineers, 2nd ed., p. 205, D. Van Nostrand Co., Inc., Princeton, New Jersey, 1962.

11. R. Phillips, "An Analysis of the Influence of Some Minor Alloy Additions on the Mechanical Properties of Mild Steel," ISI Special Report 81, 1963, pp. 36-40.

12. I. M. MacKenzie, "Niobium Treated Carbon Steels," ISI Special Report 81, pp. 30-35.

13. W. B. Morrison, "The Influence of Small Niobium Additions on the Properties of Carbon-Manganese Steels," Journal of the ISI, 1963, Vol. 201, pp. 317-325.

14. N. J. Petch, "The Ductile-Clevage Transition in Alpha-Iron," A Symposium Held at the Massachusetts Institute of Technology, June 1950: Fatigue and Fracture of Metals, W. M. Murray, ed., pp. 54-67, John Wiley & Sons, Inc., New York, 1952.

15. T. Gladman, "Discussion," ISI Special Report 81, p. 42.

16. W. E. Duckworth, "Discussion," ISI Special Report 81, p. 23.

17. L. Zadorozhnaya, N. I. Sandler, Sh. R. Dobruskina, and É. I. Fel'dman, "Effect of the Carbon and Manganese Concentrations on the Properties of Low-Alloyed Steel Containing Small Amounts of Niobium," Metal Science and Heat Treatment, 1965, No. 11, pp. 727-729.

18. J. M. Gray and R. B. G. Yeo, "Columbium Carbonitride Precipitation in Low-Alloy Steels with Particular Emphasis on 'Precipitate-Row' Formation," American Society for Metals Transactions Quarterly, 1968, vol. 61, pp. 255-269.

19. J. W. Spretnak, "Discussion," ASM Trans. Quart., 1968, Vol. 61, pp. 851-852.

20. E 206-66, 1971 Annual Book of ASTM Standards, Part 31, pp. 580-585.

21. Batelle Memorial Institute, Prevention of the Failure of Metals Under Repeated Stress, p. 107, John Wiley & Sons, Inc., New York, 1941.

22. F. A. D'Isa, Mechanics of Metals, p. 322, Addison-Wesley Publishing Company, Reading, Massachusetts, 1968.

23. J. T. Ranson and R. F. Mehl, "The Statistical Nature of the Fatigue Properties of SAE 4340 Steel Forgings," ASTM Special Technical Publication No. 137, p. 3, 1952.

24. P. Beardmore and C. E. Faltner, "Directionality of Fatigue Properties in a Low Carbon Alloy Steel," Metallurgical Trans., 1970, Vol. 1, p. 1472-1474.

25. R. C. Boettner, "Fatigue Crack Nucleation in a High-Strength Low-Alloy Steel," Trans. of the Metallurgical Society of the American Institute of Mining, Metallurgical and Petroleum Engineers, 1967, Vol. 293, pp. 1030-1033.

26. A. M. Aksoy, "Discussion," ASM Trans. Quart., 1957, Vol. 49, pp. 514-515.

27. N. Thompson, "Experiments Relating to the Basic Mechanisms of

Fatigue," Proceedings of the International Conference on Fatigue of Metals, 1956, p. 527-530.

28. J. R. Low, Jr., Progress in Materials Science Volume 12: The Fracture of Metals. Pergamon Press Limited, New York, 1963, p. 47.

29. Low, p. 41.

30. J. E. Grosskreutz, Proceedings of the 10th Sagamore Army Materials Research Conference: Fatigue--An Interdisciplinary Approach, Syracuse University Press, Syracuse, New York, 1964, p. 27.

31. K. R. L. Thompson, T. Araki and I. Uchiyama, "Fatigue Fracture in a High-Strength Low-Alloy Steel," Journal of the ISI, 1969, Vol. 207, p. 1624-1627.

32. N. Thompson, N. J. Wadsworth and N. Louat, "The Origin of Fatigue Fracture in Copper," Philosophical Magazine, 1956, Series 8, Vol. 1, pp. 113-126.

33. M. R. Hempel, "Slip Band, Twins and Precipitation Processes in Fatigue Testing," Proceedings of an International Conference on Atomic Mechanisms of Fracture: Fracture, B. L. Averbach, et. al., eds, John Wiley & Sons, Inc., New York, 1959, pp. 412-434.

34. H. Nordberg and B. Aronsson, "A Microfractographic Investigation of Fatigue Cracks in a Low Alloy Cast Steel," ASM Trans. Quart., 1968, Vol. 61, pp. 627-629.

35. R. C. Boettner, C. Laird, A. J. McEvily, Jr., "Crack Nucleation and Growth in High Strain-Low Cycle Fatigue," Trans. of TME - AIME, 1965, Vol. 233, pp. 279-387.

36. A. Bush, Proceedings of an International Conference Held in Warsaw: Fatigue Resistance of Materials and Metal-Structural Parts, A. Bush, ed., Pergamon Press Limited, Oxford, England, 1964, pp. 3-32.

37. Low, p. 38.

38. Prevention of the Failure of Metals Under Repeated Stress, p. 87.

39. J. C. Levy and G. M. Sinclair, "An Investigation of Strain Aging in Fatigue," Proc. of ASTM, 1955, Vol. 55, pp. 866-870.

40. T. Kawasaki, H. Izumi, Y. Sawaki, "A Theoretical Explanation for the Increase in Fatigue Strength of Mild Steel at Elevated Temperatures," ASM Trans. Quart., 1967, Vol. 60, pp. 707-711.

41. R. K. MacCrone, R. D. McCammon, and H. M. Rosenberg, "The Fatigue of Metals at 1.7°K," Philosophical Magazine, 1959, series 8, Vol. 4, pp. 267-268.

42. A. J. Kennedy, Processes of Creep and Fatigue in Metals, John Wiley & Sons, Inc., New York, 1963, pp. 368-370.

43. P. L. Teed, "The Influence of Metallographic Structure on Fatigue," A Symposium Held at the Massachusetts Institute of Technology, June 1950: Fatigue and Fracture of Metals, W. M. Murray, ed., John Wiley & Sons, Inc., New York, 1952.

44. G. H. Rowe, "Discussion," Proc. of 10th Sagamore Army Conference, pp. 22-23.

45. A. Esin, "The Microplastic Strain Energy Criterion Applied to Fatigue," Transactions of the American Society of Mechanical Engineers, Journal of Basic Engineering, No. 3, 1968, pp. 28-36.

46. K. J. Irvine, "The Development of High-Strength Structural Steels," ISI Publication 104, pp. 1-10.

47. High Strength Low Alloy Steels, Republic Steel Corporation, Cleveland, Ohio, 1971, p. 21.

48. Republic Steel Message, 0012 0913, Gadsden, Alabama, March 8, 1972.

49. W. E. Duckworth, "Thermomechanical Treatment of Metals," Journal of Metals, Vol. 18, No. 8, 1966, pp. 915-922.

50. J. J. Irani and D. J. Latham, "Applications of Isoforming and Allied Treatments to Low-Alloy Steels," ISI Publication 114, 1968, pp. 55-64.

51. S. A. Andrew, Mechanical Behavior of Thermomechanically Treated X-60 Steel, Master's Thesis, Georgia Institute of Technology, 1972.

52. Manual on Fatigue Testing, ASTM Special Technical Publications No. 91, 1949, pp. 3-5.

53. A. R. Rosenfield, E. Voltava, G. T. Hann, "Slip-Induced Crack Formation in Mild Steel," ASM Trans. Quart., 1968, Vol 61, pp. 807-815.

54. J. T. Boyd, G. T. Hann, A. R. Rosenfield, and E. Voltava, "Character of Slip Bands in Iron and a Milk Steel with Manganese," ASM Trans. Quart., Vol. 62, 1969, pp. 206-218.

55. A. T. Davenport, Republic Steel Research Center, private communication, June 1972.